Effect of Ti & Al addition on the mechanical properties of Cu-Zr based metallic glasses: A molecular dynamic simulation study

A thesis submitted in partial fulfilment of the
requirements for the degree of

Master of Technology

In

Metallurgical and Materials Engineering

By

Ajnish Kumar

(Roll No-211MM1361)

Department of Metallurgical and Materials Engineering

National Institute Of Technology, Rourkela

May 2013

Effect of Ti & Al addition on the mechanical properties of Cu-Zr based metallic glasses: A molecular dynamic simulation study

A thesis submitted in partial fulfilment of the
requirements for the degree of

Master of Technology

in

Metallurgical and Materials Engineering

By

Ajnish Kumar

(Roll No-211MM1361)

Under the guidance and supervision of

Prof. Natraj Yedla

Department of Metallurgical and Materials Engineering
National Institute Of Technology, Rourkela
May 2013

Dedicated

To

My Parents

&

Family

National Institute Of Technology

Rourkela

CERTIFICATE

This is to certify that the thesis entitled, "**Effect of Ti & Al addition on the mechanical properties of Cu-Zr based metallic glasses: A molecular dynamic simulation study"** submitted by **Ajnish Kumar (211MM1361)** in partial fulfilment of the requirements for the award of Master of Technology in **Metallurgical and Materials Engineering** at the National Institute of Technology, Rourkela is a bonafide research work carried out by his under my supervision and guidance.

To the best of my knowledge, the matter embodied in the thesis is based on candidate's own work, has not been submitted to any other university / institute for the award of any degree or diploma.

Date:

Place:

Dr. Natraj Yedla

Assistant professor

Dept. of Metallurgical and Materials Engineering

National Institute of Technology

Rourkela – 769008

ACKNOWLEDGEMENTS

This work would not have been possible without the support from **NIT, ROURKELA**. I want to express my outmost gratitude to my supervisor, **Dr. N. YEDLA**, for their support, both intellectual and emotional, throughout the years of my M.TECH studies. They have taken me from my infantile knowledge of materials science and introduced me to a whole new world. Performing experiments with them left me in both joy and awe and I hope to retain this excitement in any future research endeavour. It was through their encouragement and understanding that I am standing here today, about to embark on a career in academia. I want to thank them for all the time they have spent with me explaining the most obscure concepts, for helping me view results with a whole new light and for teaching me how to think by myself. I hope that one day I may be able to repay them for all the good they have done for me.

I would also like to express our utmost gratitude to **Prof. B.C Ray, HOD, Metallurgical & Materials engineering** for allowing us to use the departmental facilities and for his valuable suggestions and encouragements at various stages of the work.

I also want to thank my friends who have always encouraged and supported in doing our work. I would like to thank all the staff members of Department of Metallurgical &Materials Engineering who have been very cooperative with us.

Finally, I would like to express my deepest gratitude to my parents for their unconditional love and encouragement. I would not be where I am today without the support of them.

Ajnish Kumar (211MM1361)
Metallurgical & Materials Engineering
NIT, Rourkela

Abstract

This thesis presents research using molecular dynamics (MD) simulation techniques to study the mechanical properties of Cu-Zr based metallic glasses. Classical molecular dynamics simulation deformation studies of Cu-Zr (Al, Ti) metallic glasses were performed. The MD simulations were coded in LAMMPS. Owing to the brittle nature of $Cu_{50}Zr_{50,}$ the effect of Al (2 at% and 10 at % respectively) & Ti (2 at% and 6 at % respectively) on the mechanical properties was studied. Addition of Al and Ti significantly improved the mechanical properties of $Cu_{50}Zr_{50}$ glassy alloy. Mechanical properties were evaluated by subjecting the model alloys to uniaxial tensile deformation at varying strain rates and temperature. It was found that alloys were sensitive to strain rate. There are three strain rates (1×10^{10}, 2×10^{10} and 4×10^{10} S^{-1}) at which MD simulations have been done. Also uniaxial tensile deformation has been done at two different temperatures (300K & 500K).

Keywords: Metallic glasses, Molecular dynamics, LAMMPS, Strain rate.

Contents

List of Figures

List of Tables

Chapter 1
Introduction

1.1 Background

Metallic glass was first synthesized in the year 1960, at California Institute of Technology. Duwez et al. [1] discovered the first binary metallic amorphous alloy $Au_{80}Si_{20}$. They used the process of rapid quenching techniques for cooling the liquid metals at very high rates approximately 10^6 K/s. Due to this cooling rate there is no enough time to rearrange for crystal nucleation and the material is frozen in an amorphous state. The atoms hang on an amorphous distribution, for this reason they have no long-range order. Owing to lack of long range order metallic glasses possess exclusive mechanical properties which make them smart materials for fabricating components for range of applications. For example, the industrial Zr-based metallic alloys reveal a reasonably high young's modulus (~ 90 GPa), high tensile strength (2 GPa), high yield strain (2%) , good fracture toughness (10-50 MPa$\sqrt{m}$), and good wear resistance. A main important characteristic of metallic glasses is their intrinsic homogeneity to the nanoscale because of the lack of grain boundaries. This characteristic coupled with their exceptional mechanical properties, makes them perfect materials for fabricating micron- scale components. For example, as dies for manufacture of polymeric micro fluidic devices [2]. Metallic glasses show inimitable characteristic that is, absence of transitional periodicity and compositional homogeneity [3].

When metallic glasses are deformed at room temperature their inelastic deformation is characterized by strain-softening, which results in the formation of intense localized shear bands. Fracture typically occurs after very small inelastic strain levels which can be achieved under states of confined compression, such as in indentation experiments. The promising attributes of metallic glasses have led metallurgists to the vision of new alloys that would form glasses at low cooling rates like oxide glasses, which would facilitate their production in bulk form [4]. The bulk glassy alloys show high tensile fracture strength of 2000–2160 MPa, compressive fracture strength of 2060–2150 MPa and compressive plastic elongations of 0.8–1.7%. The result of the new Cu-based bulk glassy alloys with high GFA, high fracture strength above 2000 MPa and different plastic elongation is encouraging for the future development of a new type of bulk glassy alloy which can be used for structural materials [5]. General deformation characterization of Cu-Zr based metallic glasses; both in tensile and compressive mode have been carried out to investigate the possibility of room temperature ductility in these metallic glasses [6, 7, 8, 9]. Some studies claim that the presence of

crystalline phase decreases the ductility [10]. In the deformation studies by compression, [11] they have shown that the addition of Ti to Cu-Zr glass promotes crystallization and hence enhances the plasticity. The addition of Al to Cu-Zr glass has been also found to significantly enhance the ductility [12, 13].

1.2 Research objectives

(a) To study the Effect of Ti & Al addition on the mechanical properties of Cu-Zr based metallic glasses.

(b) To study the effect of strain rate on the tensile deformation behavior of binary (Cu-Zr), and ternary (Cu-Zr-Al/Ti) alloys.

(c) To study the effect of temperature on the tensile deformation behavior of binary (Cu-Zr), and ternary (Cu-Zr-Al/Ti) alloys.

****

Chapter 2

Literature Review

2 Literature review

2.1 Introduction

When the liquid phase cooled to below its freezing temperature, transformed into a solid called crystalline solid. Some liquid do not crystallize because of complex molecular configuration or slow molecular transport, but instead form a rigid disordered network known as glasses which is very similar structure to that of the liquid. A glass or an amorphous material is a disordered solid which has short range periodicity not like as a typical crystal. A glass is obtained by rapid cooling from the liquid and is formed when the liquid becomes increasingly viscous during cooling and fails to crystallize. Glass forming ability is the ease with which crystallization can be avoided and thus make a glassy state of material from its liquid state upon cooling [14]. So glasses are vitrified liquids which are having disordered atomic arrangement. Fig.1 shows the schematic of atomic arrangements in crystals and that of glasses [15].

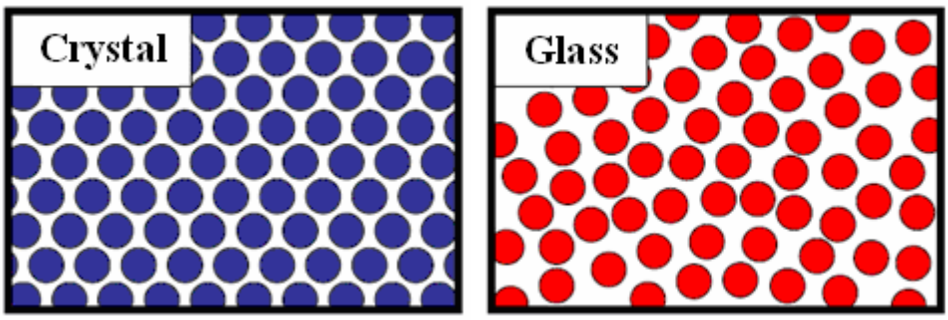

Fig. 2.1: Atomic arrangement of crystal and glass structure [15].

2.1.1 The glass transition

Generally glass formation is quenching process in which liquid change into solid state while formation of crystal is kinetically suppressed. When the liquid passes its melting point T_m without crystallization is called supercooled liquid (SCL). SCL is having different properties from regular liquids and with decreasing temperature the system dynamics can slow by more than 20 orders of magnitude within only a few Kelvin. The temperature dependence on liquid's volume at constant pressure is shown in Fig. 2.2 [16, 17]. When cooling takes place below the melting point T_m, the motion of molecules slow down. If the

cooling rate of liquid is too fast, crystallization will be suppressed and results in the hindrance of rearrangement of molecules [18, 19]. This falling out of equilibrium occurs across a narrow transformation range where the time of relaxation is the order of 100 seconds and the rate of change of enthalpy or volume with respect to temperature decreases rapidly as compared to the crystalline solid. The resulting structures are called glasses. In Fig. 2.2 the intersection point of liquid and glass curve called glass transition temperature, T_g which is equal to $2T_m/3$ approximately. With increasing cooling rate the onset of glass transition increases [20, 21].

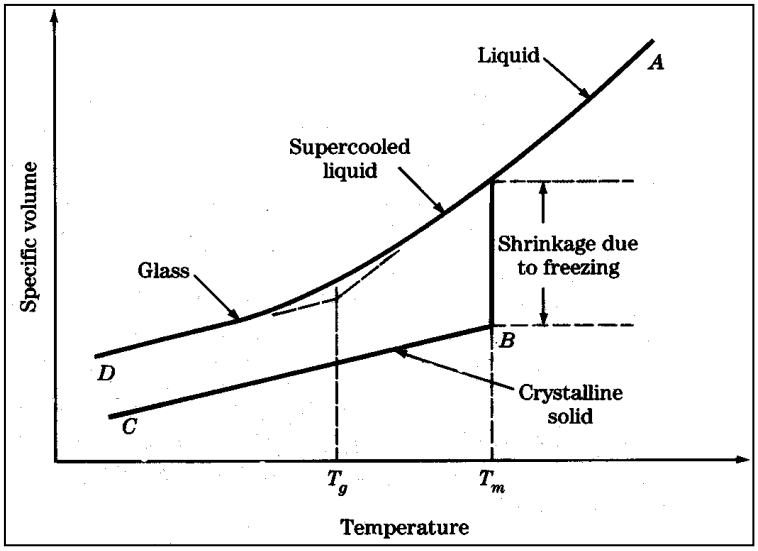

Fig. 2.2**:** Volume-temperature plot showing the relationships between liquid, glassy and solid states

2.2 Metallic Glasses

With the help of rapid quenching methods such as vapour condensation, electrodeposition, chemical deposition, and rapid liquid quenching the liquid structure can be retained for many metals and alloys [22]. Amorphous metallic alloys represent a young class of materials which has been developed in 1960 by Klement et al. an experiment on Au-Si alloys [23]. BMGs have been formed in various multi-component alloys. As BMGs bulk metallic glasses are applicable to structural materials, their mechanical properties have become a matter of great interest. Metallic glasses with various features and which make them different from crystalline alloys, ceramic crystals and other kinds of glasses are discussed below [23, 24]:

- *Localized shear deformation*: Generally inorganic glasses are brittle in nature at room temperature, and have a smooth fracture surface. On the other hand metallic glasses generally deform by localized shear deformation (LSD) at room temperature and also ductile in nature when bending and rolling deformation are takes place. Under uniaxial tension metallic glasses undergo shear fracture immediately just after the yielding without showing appreciable microscopic plastic strain. Thus, metallic glasses are normally not brittle at microscopic level but at microscopic level they are not ductile for both tension and compression. Fig. 2.3 shows an example of yield stress under the uni-axial tension of Cu-Zr binary metallic glasses depend over a wide range of temperature [25].

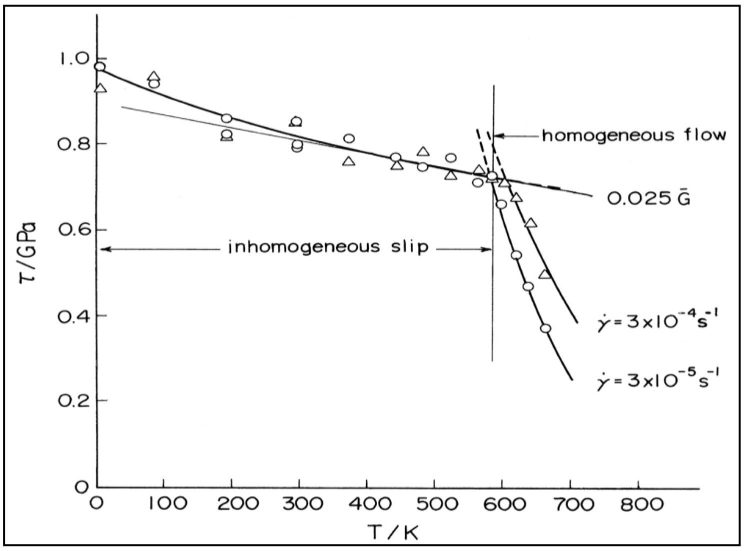

Fig. 2.3: Temperature dependence of critical resolved shear stress of ribbon samples of $Cu_{57}Zr_{43}$ metallic glass.

Above the critical temperature and near the glass transition temperature metallic glass samples exhibit homogeneous viscous flow with yield stress being quite strain-rate sensitive, that's by critical temperature is strain-rate dependent. Below the critical temperature, generally these glasses deform plastically by LSD.

- *Homologous nature*: Fig. 2.4 shows the relation between the Vickers hardness value (H_v) and Young's modulus (E) at room temperature for various metallic glasses in the form of ribbons and bulk samples for various alloy systems..We can relate the H_v and E with the help of following equation

$$H_V = 0.06E \quad \text{.......} \quad (1)$$

Above correlation is first noted by Whang et al. [26]. There is also a correlation between yield stress σ_y and Young's modulus E as

$$\sigma_y = 0.02E \quad \ldots\ldots\ldots\ldots\ldots\ldots\ldots\ldots\ldots\ldots\ldots\ldots\ldots\ldots\ldots\ldots\ldots\ldots \quad (2)$$

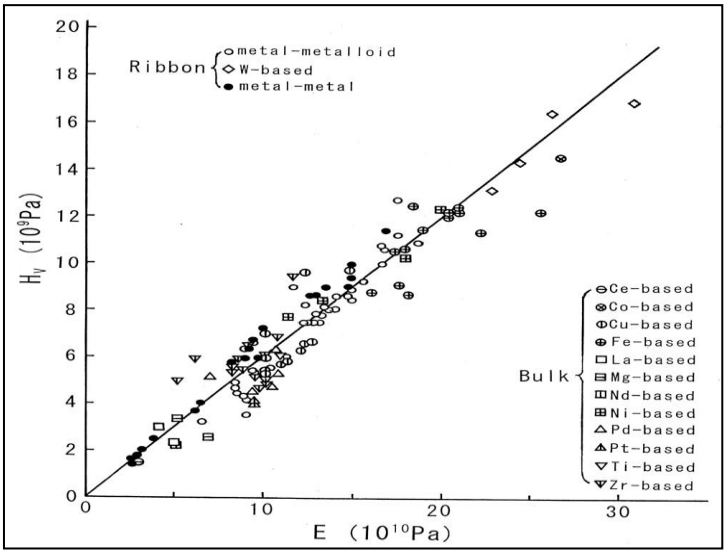

Fig. 2.4: Relation between Vickers hardness and Young's modulus of various metallic glasses.

From Eq. (2) it can be seen that the yield stress is almost same in any metallic glasses and elastic strain limit (2%) which is greater than crystalline alloys.. Third relationship is obtained from the combination of Eq. (1) and Eq. (2) As $H_v = 3\sigma_y$ indicates the metallic glasses are ideal plastic solid having a constant flow stress [26]. The homologous nature expressed by Eqs. (1) and Eqs. (2) on the strength of metallic glasses suggest that the mechanism of shear band deformation is largely common for any kind of metallic glasses.

Although metallic glasses are having desirable mechanical properties, their mechanism of yielding and failure is still not thoroughly understood. It is reported that at ambient temperature the process of deformation of metallic glasses is "shear banding" where plastic strain is highly localize into strips of nanometer thickness and macroscopic length. The performance of shear bands on the nanometer scale gives rise to unique mechanical properties at macroscopic scales. As for example, the very low values of tensile elongation has been seen for amorphous metals are assign to rapid failure along single shear band. In different modes of loading like indentation or compression, plastic yielding is observed, but it does not takes place smoothly, instead exhibiting "load serrations" during long intervals

when the strain is carried by a single shear band. These unique properties have been seen in a variety of glassy alloys with different composition. BMGs have also attracted owing to their large elastic limit. However, the room temperature brittleness and strain-softening nature limit their real structure applications. Among many ideas and their implementation was to be done to overcome this issue, forming BMG-matrix composite has effective compressive plasticity and toughness [27]. By proper adjusting dendrite spacing through controlling preparation route tensile ductility had been absorbed by Johnson et al. [28, 29]. They were achieving large tensile ductility in Zr and Ti based BMG composites. But even after this research BMG composite suffer from macroscopic strain softening with neck formation near yield point due to lack of work-hardening mechanism. For engineering application work-hardening capability and uniform tensile ductility are necessary, so addition of ternary elements such as Al, Ti, Ag to Cu-Zr-based alloy has been researched which enhance the glass forming ability significantly. Among these alloys the Cu-Zr-Al system are good material for engineering purpose because this alloy has good thermal stability, good combination of strength and ductility and relatively low production cost. Apart from this, the Cu-Zr-Al system provides a unique opportunity to toughen BMGs through ductile intermetallic phase, which is harder due to martensitic transformation. In Cu-Zr system intermetallic compound with an austenite or martensite like structure improves their plasticity; however the deformation mechanism of martensitic phase during tensile loading is still unclear [30]. A characteristic feature of plastic deformation of metallic glasses at the ambient temperature is the localized shear deformation. Since we have no appropriate experimental technique, unlike crystalline matter, to approach microscopic deformation process in amorphous materials, we have to faith on computer simulation studies by use of atomistic models to reveal the microscopic deformation processes.

2.3 Deformation mechanism of metallic glasses

Generally amorphous alloys having metallic bonding and strain can be easily readable at the atomic level due to changing in position of different molecules. That means atomic bonds can be broken and again reform at atomic scale. We know that metallic glasses have short-range bond unlike crystalline metals. Also dislocations allow changes in atomic arrangement at low energy and stresses in crystals, whereas in glasses relatively stresses and energy are high [23]. In this topic we cover the mechanism of plastic flow in metallic glasses. In metallic glasses strains are generated due to shear transformations nucleated due to applied

stresses and also due to thermal fluctuations which takes place around the sites of free volume of the glassy structure. With the help of an atomic-anlog bubble-raft model Spaepen and Argon explained the deformation mechanism of metallic glasses [31, 32]. Fig.2.5a shows the mechanism of plastic flow in metallic glasses [31]. Fig. 2.5b is a free-volume model which was developed by Turnbull et al. [33]. This method shows that how an atomic jump takes place in the glasses. These jumps help the neighbour sites which are having high free volume. This event is described as a "flow" defect or "a local inelastic transition" and increasingly commonly a "shear transformation zone (STZ). The STZ consist of cluster of atoms which is cause of inelastic shear distortion from low energy configuration to high energy configuration.

As per Argons theory the flow can localize in a band in which the strain rate has been distracted, when the threshold stress operate the local shear transformation is changed through creation of free volume. So, we can say that the Argon's model explains the inhomogeneous deformation.

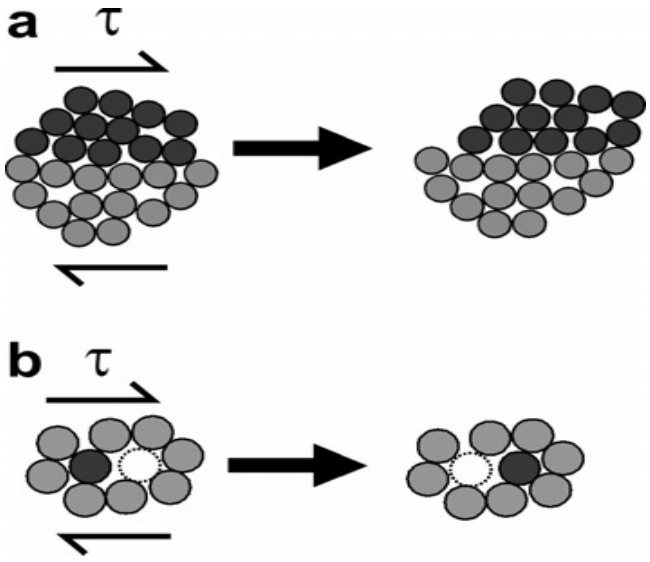

Fig. 2.5: Two-dimensional schematics of the atomistic deformation mechanisms proposed for amorphous metals, including (a) a shear transformation zone (STZ) [31] and (b) a local atomic jump [32]

2.3.1 Plastic deformation

There are various theories describing the plastic deformation behaviour of metallic glasses. The strain-accommodation local rearrangement theory was purposed by Argon. According to Argon, in plastic deformation strains are produced due to local shear

transformations which are nucleated when the stresses are applied and distribution of thermal fluctuation are around the free volume sites of the glassy structure [31]. As per Spaepen [32] the deformation behavior in metallic glasses is a strong function of temperature and stress. Fig. 2.6 is the deformation mechanism map of metallic glasses in which the solid lines are the strain rates line which are independent of temperature i.e. strain rates are constant. Metallic glasses above the liquid temperature T_{liq} behaves like a Newtonian fluid. Viscosity increases at very fast rate with cooling of the liquid. In temperature range between T_x and T_g deformation is a strong function of applied strain rate which is shown in Fig. 2.6.

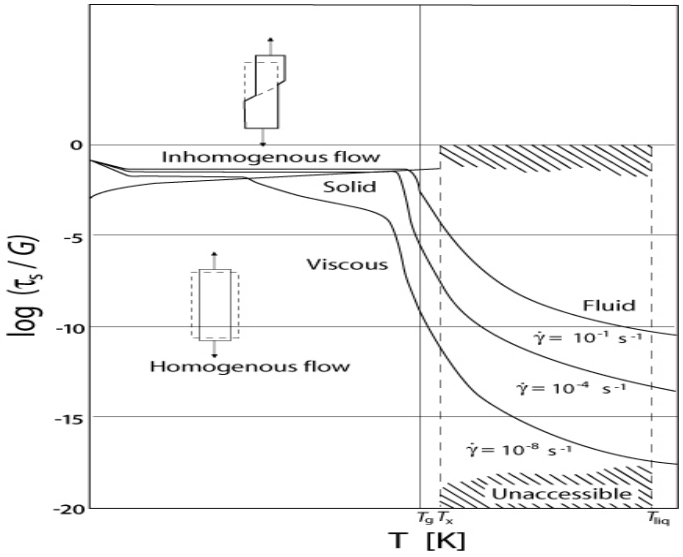

Fig. 2.6: Deformation map of metallic glasses [32]

Deformation is of two types, homogeneous and inhomogeneous deformation depending on the temperature. The following sections discuss these in detail.

2.3.2 Homogeneous deformation

Generally homogeneous deformations takes place near about the glass transition temperature and it depends on the strain rate. If strain rates are low, it behaves like as Newtonian fluid while its nature is non-Newtonian when the strain rates are high and consequences are Microstructural instability. Homogeneous deformation of metallic glasses is divided into three regions namely [34] a) deformation occurring below T_g, b) between T_g and T_x (crystallization temperature) and c) above T_x.

- *When $T < T_g$*: In the creep test studies (Mulder et al.) on $Fe_{40}Ni_{40}B_{20}$ metallic glass at elevated temperature 523 and 548 K which is below the glass transition temperature (700 K) and applied stress (>1.0 GPa) it was concluded that activation energy is approximately equal to eutectic crystallization below the glass transition temperature.

Kawamura et al. [36] studied the deformation properties of glass $Zr_{65}Al_{10}Ni_{10}Cu_{15}$ whose T_g and T_x are respectively 652 K and 757 K. After the study they found that the strain rate sensitivity of this alloy is low (m < .25) and tensile elongation is also low (< 100%). From the above results we may conclude that the deformation of metallic glasses near the temperature T_g are characterized by a low strain rate sensitivity and ductility.

- *When $T < T_x$*: Generally metallic glass alloys are crystallized and form nanocrystalline structure above the T_x. At temperature T material are not exist in amorphous form but rather nanocrystalline. Researchers are not able to get more information of deformation of metallic glasses above the temperature T_x. Kawamura et al. [36] explain that the ductility of a BMGs are generally large in the supercooled liquid region but drastically reduces over the T_x .
- *When $T_g < T < T_x$*: This region is called supercooled liquid region. Khonik and Zelenskiy [37] had found out some mechanical data after the study of 15 different metallic glasses, they found that if the value of ΔT is large superplasticity occurs in metallic glass alloys, where $\Delta = T_x - T_g$ .if ΔT is larger, tensile elongation is also large. They also propose that with increase in rate of heating elongation is larger. Since faster rate of heating and larger value of ΔT minimizes the crystallization during superplastic deformation. Table 2.1 shows the mechanical and thermal properties of metallic glasses.

Table 2.1: Deformation data of some bulk metallic glasses in the supercooled liquid region [34].

Alloy (in at. %)	Tg(k)	Tx (k)	m value	Ductility
La55Al25Ni20	480	520	1	1800 (T)
$Zr_{65}Al_{10}Ni_{10}Cu_{15}$	652	757	0.8-1	340 (T)
$Pd_{40}Ni_{40}P_{20}$	578-597	651	0.4-1	1260 (T)
$Zr_{55}Cu_{30}Al_{10}Ni_5$	683	763	0.5-1	Nil (c)
$Pd_{40}Ni_{40}P_{20}$	589	670	0.5-1	0.94 (c)

$Zr_{65}Al_{10}Ni_{10}Cu_{15}$	652	757	0.83	750 (T)
$Zr_{55}Al_{10}Cu_{30}Ni_{5}$	670	768	0.5-0.9	800 (T)
$Cu_{60}Zr_{20}Hf_{10}Ti_{10}$	721	766	0.3-0.61	0.78 (C)
$Zr_{52.5}Al_{10}Cu_{22}Ti_{2.5}Ni_{13}$	659	761	0.5-1	> 1.0 (C)
$Zr_{52.5}Al_{10}Ti_{5}Cu_{17.9}Ni_{14.6}$	358	456	0.45-0.55	650 (T)
$Zr_{41.25}Ti_{13.75}Ni_{10}Cu_{12.5}Be_{22.5}$	614	698	0.4-1	1624 (T)
$Ti_{45}Zr_{24}Ni_{7}Cu_{8}Be_{16}$	601	648	Nil	1.0 (T)
$La_{60}Al_{20}Ni_{10}Co_{5}Cu_{5}$	451	523	1.0	Nil

Here ‘T’ and ‘C’ stands for tension and compression.

2.3.3 Inhomogeneous deformation

Generally the reason of inhomogeneous deformations is non-uniform distribution of free volume, which is coming from quenching process or thermal fluctuation. At low temperature (< Tg) deformation is inhomogeneous and is carried by narrow shear band, highly localized, limiting macroscopic plasticity. In tension, plastic deformation is very low due to this shear band develops, which leads to fracture of the material. Serrated plastic flow is observed during this deformation in different loading modes like-compression, bending, and tearing. The main causes of inhomogeneous deformation are shear bands and serrated elastic flow. These two properties are strong function of strain rates [38].

2.3 Properties & Application of metallic glasses

2.4.1 Properties of metallic glasses

Generally, metallic glasses have no plasticity at room-temperature. Because of this they have limited applications in industries and structural work. However, some unique properties of metallic glasses make them attractive for other type of glasses. Some applications of metallic glasses are explain below [39]:

- *Basic characteristic of glassy alloy*: Fig. 2.7 explains the relationship between tensile strength and Young's modulus for glassy alloy. In this glassy alloy shows the unique mechanical properties comparison to crystalline materials like-
  - Tensile strength is higher in metallic glasses. It is approximately three times higher than that of crystalline alloys for the same young's modulus.
  - The young's modulus of glassy alloy is one third as high as comparison to crystalline materials for the same tensile strength.
  - Glassy alloy holds good relationship between tensile strength & young's modulus. They follow Hook's law. The elastic elongation limit in glassy alloy is about 2% which is approximately three times larger than that for crystalline materials (approx 0.65%).
  - The shear stress under a torsional deformation is approximately three times larger than that of crystalline materials.

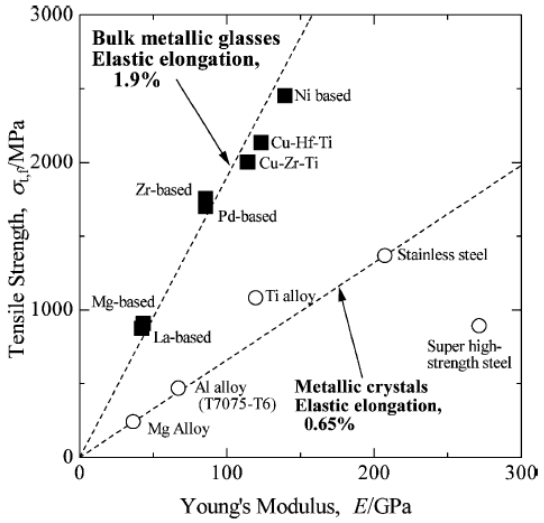

Fig. 2.7: Plot of tensile strength vs young's modulus for typical transition metal glassy alloy.

- *High Ductility of Bulk Glassy Alloys by Coexistence with Crystalline Phase*: Glassy alloy can have high yield strength and ductility. For example Fe-based composite bulk glassy alloys having improved soft magnetic properties in case of nanoscale α-iron phase dispersion state and hard magnetic properties in case of *nanoscale* bct-FePt phase dispersion state.
- *Formation of Porous Bulk Glassy Alloys*: If ductility to be increases, then some mechanical properties like-young's modulus, strength, and specific weight of porous glassy alloys are decreases but energy absorbing capacity is increasing up to fracture.

These alloys contain the spherical pores with sizes about 15 to 33 μm in wide volume fraction range. The 0.2% proof stress and young's modulus as a function of porosity can be found by the taking effects of stress concentration around pores. Due to high ductility, high energy absorbing capacity, and low stiffness its future application field are broad.

- *Production of Glassy Alloys in Various Forms of rod, Plate and Ball*: At present time there are different casting techniques to produce glassy alloy with demandable shape to fulfil the requirement in engineering application. So we can use the glassy alloy as rod, sheets, and spherical balls (Fig. 2.8).

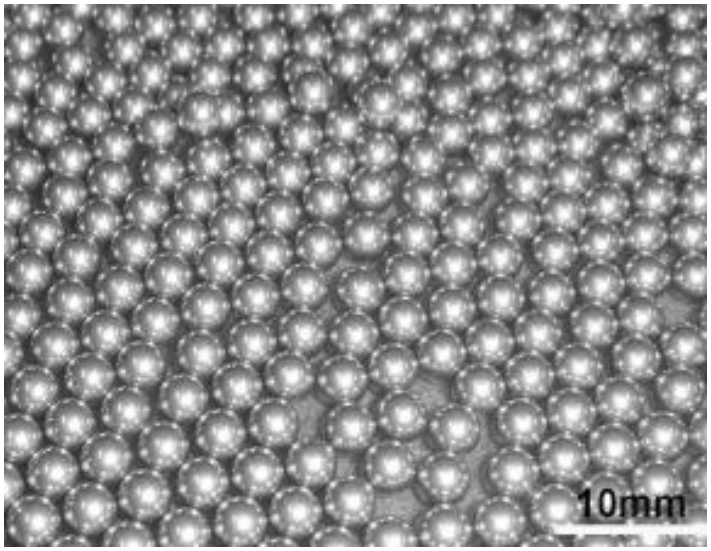

Fig. 2.8: glassy alloy balls with 3 mm diameter

- *Unique Working Processes*: Metallic glasses display the glass transition temperature after that supercooled liquid and then crystallization reaction when heat regularly. We get Newtonian flow characteristic in the supercooled region. As we know that the value of strain rate sensitivity exponent (m) for Newtonian fluid is 1.0 that means it indicates the stage of ideal super plastic. Due to these properties we can elongate it at high percentage. By the use of Newtonian flow characteristic we can produce a surface at nano level (about 22 nm) by the process of pressing treatment in supercooled liquid region. Due to these outstanding properties, these alloy have much interest as an advance materials for nanotechnology process.

2.4.2 Applications of metallic Glasses

- Cellular phone casing
- Shot penning balls

- Electromagnetic shield plates
- High torque geared motor parts
- Connecting part for optical fibres
- Various shape of optical mirrors
- Electromagnetic sliding plates
- High corrosion resistance coating plates
- Vessels for lead free soldering
- Casing in electromagnetic equipments

2.5 Additional details about Cu-Zr based metallic glasses

2.5.1 Effect of Ti and Al alloying elements on the mechanical properties of Cu-Zr metallic glasses

Studies on the effect of Al and Ti additions on the mechanical properties of the Cu-Zr metallic glasses (Das et al., 2005; Pauly et al., 2007; Yu and Bai, 2007) showed that addition of third element to the binary Cu-Zr system improved the GFA, yield strength and plasticity. These studies were summarized in Table 2.3. Addition of 5 at. % Al significantly increased the plastic strain with work hardening behavior and Ti content <7.5 at. % promoted crystallization. However, the mechanical properties depend on whether the structure is fully glassy and also on the volume fraction of the crystallizing phases.

Table 2.2: Effect of Al and Ti alloying elements on the mechanical properties of Cu-Zr bulk metallic glasses tested under compression [40]

Alloy	x, at. %	Yield strength (MPa)	Plastic strain ε_p (%)	Fracture strain ε_f (%)	Young's Modulus E (GPa)
$(Cu_{50}Zr_{50})_{100-x}$	0	1272	6.2	7.9	87.0
	5	1547	15.0	18.0	88.7
	6	1100	2.0	3.5	92.4
	8	1200	1.4	2.9	93.7
$Cu_{50}Zr_{50-x}Ti_x$	2.5	1495	12.5	14.6	79.6
	5.0	1350	13.3	15.3	79.0
	7.5	1718	11.1	13.4	81.5

2.5.2 Effect of strain rate

Room temperature compressive studies on 2 mm diameter $Cu_{47}Zr_{47}Al_6$ bulk glassy alloy at strain rates 2.5×10^{-4} s^{-1} and 8×10^{-5} s^{-1}indicated that yield strength and plastic strain increased with increase in strain rate (Duhamel et al., 2008). On the other hand, Hajloui et al. (2008) showed that yield strength and elastic strain limit decreased with increase in strain rate from 10^{-3} s^{-1} to 2×10^{-5} s^{-1} during the tensile deformation behavior of $Zr_{55}Cu_{20}Ti_5Al_{10}Ni_{10}$ bulk metallic glass. Table 2.4 summarizes the mechanical properties of the above studies.

Table 2.3: Effect of strain rate on the mechanical properties of $Cu_{47}Zr_{47}Al_6$ and $Zr_{55}Cu_{20}Ti_5Al_{10}Ni_{10}$ BMGs at 300 K under compression and tensile [40]

Alloy composition	Dimension mm	Strain rate	σ_y MPa	σ_f MPa	ε_p	ε_f
$Cu_{47}Zr_{47}Al_6$	ø 2 × 4	2.5×10^{-4} s^{-1}	1821	1853	0.36	
		2.5×10^{-4} s^{-1}	1767	1878	2.16	
		8.0×10^{-5} s^{-1}	1676	1850	4.10	
		8.0×10^{-5} s^{-1}	1603	1734	5.04	
$Zr_{55}Cu_{20}Ti_5Al_{10}Ni_{10}$	12 × 1.5 ×1	1×10^{-3} s^{-1}		1400		2.4
		2×10^{-5} s^{-1}		1600		1.8

2.5.2 Effect of temperature

The effect of temperature on stress- strain curves were studied by Lu et.al.[41]. They found that the influence of temperature on failure modes is one of the features of deformation of materials and their characterization, i.e. brittle to ductile transition. They have explained with the help of stress–strain curve in Fig. 2.9 for a strain rate of 1×10^{-1} s^{-1}. From Fig.2.9 it can be clearly seen that with increasing temperature from 295 K to 683 K yield strength decreased. At room temperature Zr41.2Ti13.8Cu12.5Ni10Be22.5 alloy exhibited the high failure stress of 1860 MPa and failed by a formation of single shear band and subsequent shear fracture. When the temperature was increased to 373 K stress decreased slightly to 1790 MPa. In the temperature range of 643- 663 K decrement of stress is maximum because of deformation mode switched from being inhomogeneous to homogeneous. In the temperature range of 663-683 K, homogeneous deformation takes place up to the strain value demonstrated on each curve.

The stress-strain curves in the homogeneous deformation region featured an increase of the initial slope as the temperature decreased, which indicates that the initial Young's modulus (or shear modulus) decreases with temperature, analogous to a similar effect in crystalline metallic alloys. Stress overshoot, the difference between peak stress and flow stress, was present at a temperature of 663 K. The cause of the stress overshoot was due to the free volume induced structural relaxation.

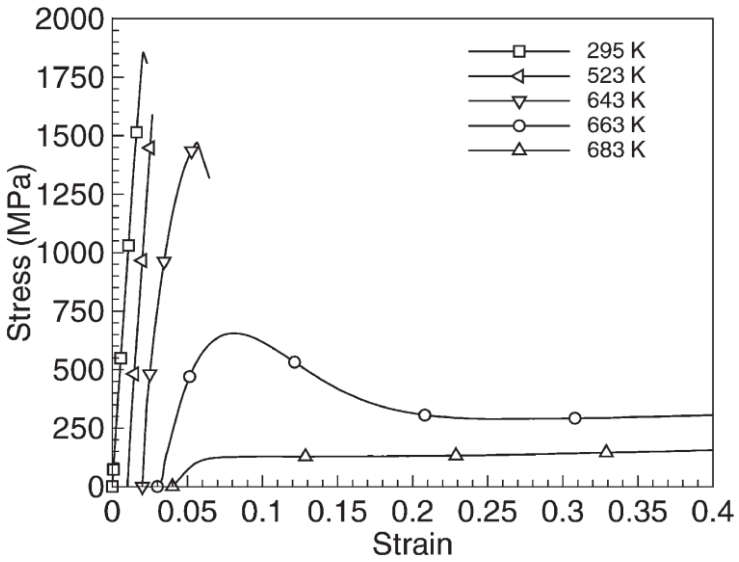

Fig. 2.9: Effect of temperature on the uniaxial stress-strain behavior of $Zr_{41.2}Ti_{13.8}Cu1_{2.5}Ni_{10}Be_{22.5}$ alloy at strain rate $\dot{e} = 1.0 \times 10^{-1}\ s^{-1}$ and temperatures T = 295, 523, 643, 663 and 683 K. The stress-strain curves have been shifted to the right to avoid overlapping curves of similar shapes and sizes.

****

Chapter 3

Theoretical & Computational Method

3. Theoretical & Computational Method

3.1 Molecular Dynamics Simulation

An atomistic simulation study consists of (1) to prepare the model of structure, (2) the deformation of the model, (3) analysis of the various molecular properties of deformation sites and their changes with plastic deformation and (4) extraction of some physical concepts concerning the deformation mechanism [42]. Atomistic simulation, due to their ability to describe the atomic-scale structures and their mechanical properties, have been a powerful technique to explore the structure-property relationship in metallic glasses of the various simulation technique presently available, the first principles calculation provide the most reliable interatomic interactions. But, in this method all calculations are based on the NVT (number of atoms, volume and temperature are constant) ensemble, which is different from condition of laboratory means just all conditions are ideal in this method. In this method also the size which taken are too small (normally less than 200 atoms) and thus produces significant statistical scatter and improper to investigate the different mechanical behavior of materials. Another method which is used called classical MD simulation. It is employing semi-empirical interatomic potentials that can manage large amount of atoms and NPT (number of atom. Pressure and temperature are constant) ensemble used [43]. In MD simulation Newton's equation is used to find the movement of atoms. For applying this equation we assume the all atoms or molecules consisted in the system and the location and velocity to be calculated numerically integrate the Newton's equation. It is an effective way to analyze the various properties of system at macroscopic level [44]. That means we can say that the aim of MD simulations of molecular systems is to compute macroscopic behaviour from microscopic interactions. Microscopic assumption consist of (1) the understanding (2) explanation of experimental result (3) semiquantitative estimates of experimental results and (4) the capability to explore the experimental data into regions, this is main difficulty in the laboratory. Some limitations in the field of molecular simulation and modeling i.e. how to configure the space which is sufficient to all possible molecular conformation for low (free) energy regions which will be consumed by a molecular system in thermal equilibrium. The other basic limitation is the calculation of a just sufficient accurate interaction energy function or force field for the molecular system of interest. The main things in MD simulation are assumptions, approximations and simplifications of the model and computational

procedure such that they contribute minimum inaccuracy means not affect significantly the property of interests [45]. When we precede the simulation with movements of atom some thermodynamic parameter of system (example- temperature, pressure, volume, and total energy) can be changes and finally we get the result. This different parameter used in various ways, which are discussing below [46]:

Micro-canonical or NVE ensemble:

In NVE ensemble adiabatic process is considered i.e. there is no heat transfer takes place. In this parameter, the system is isolated from changes in moles (N), volume (V) and energy (E). This creates a system trajectory consistent with the microcanonical ensemble. Given the initial positions and velocities we can calculate all future positions and velocities.

Canonical or NVT ensemble:

In this ensemble moles (N), volume (V) and temperature (T) are conserved. It is also sometimes called constant temperature molecular dynamics (CTMD). In NVT, the energy of endothermic and exothermic processes is exchanged with a thermostat. There are various thermostat methods are available to add and remove energy from the boundaries of the system in realistic manner.

Isothermal–Isobaric or NPT ensemble:

In NPT (also called isothermal-isobaric) ensemble, moles (N), pressure (P) and temperature (T) are conserved.

3.1.1 Basic Principles

With the help of MD simulations we can study the dynamics of atoms. It consists of the numerical and the solution of the Newton's equation of motion which may be written as [47].

$$m_i \ddot{r}_i = f_i \qquad f_i = -\frac{\delta}{\delta r_i} u \quad \ldots\ldots\ldots\ldots\ldots\ldots (3.1)$$

We need to calculate the forces f_i which are acting on the atoms. These forces are calculated from a potential energy$u(r_N)$, where r_N=$(r_1, r_2, r_3, \ldots \ldots r_N)$ represents the complete set of 3N atomic coordinates. From above equation first we find out the potential energy u. there are two cases to find out the potential energy u (1) non-bonded interactions (2) bonding potential

(1) **Non-bonded Interactions:** The potential energy $u_{non-bonded}$ represents non-bonded interactions between atoms divided into 1-body, 2-body, 3-body … terms

$$u_{non-bonded} = \sum_i u(r_i) + \sum_i \sum_{j>i} v(r_i, r_j) + \cdots \quad \ldots (3.2)$$

Where u_r represent externally applied potential field or the effects of the container walls. It is generally used for periodic simulations of bulk systems. Now, we concentrate on the pair potential $v(r_i, r_j) = v(r_{ij})$ and neglect 3-body and higher order interactions. The Lenard-Jones potential is commonly to be used in the following form:

$$v^{lj}(r) = 4\epsilon \left[\left(\frac{\sigma}{r}\right)^{12} - \left(\frac{\sigma}{r}\right)^{6}\right] \quad \ldots\ldots\ldots\ldots\ldots\ldots (3.3)$$

Where σ is diameter and r is the depth.

If electrostatic charges are present then we add the appropriate coulomb potentials

$$v^{coulomb}(r) = \frac{Q_1 Q_2}{4\pi r \epsilon_0} \quad \ldots\ldots\ldots\ldots\ldots\ldots\ldots\ldots\ldots\ldots (3.4)$$

Where Q_1, Q_2 are the charges and

ϵ_0 is the permittivity of free space.

(2) Bonding Potential: we simply build the molecules out of site-site potentials of the form of Eq. (3.3), so this study is not more interest.

Force calculation

After the find of potential we can easily calculate the force. The following step to be done for the calculation of atomic force.

$$f_i = -\frac{\partial}{\partial r_i} u(r^N) \quad \ldots\ldots\ldots\ldots\ldots\ldots\ldots\ldots (3.5)$$

3.1.2 The velocity verlet algorithm [48]

Let there are N number of particles in the system. In three dimensional vectorial representation of position, velocity and acceleration of the particles at time t are given by $r_i(t), v_i(t), \text{and } a_i(t)$ respectively. Where i $(1,2, \ldots . N)$ is the particle index and is omitted in

formula which apply to all particles independently. Vectors components are represented by subscripts x, y, z

As we know $v = {}^{dr}/_{dt}$ and $a = {}^{dv}/_{dt}$, we can write Newton's equation for the system of 6N 1st order differential equations:

$$\dot{r}_i = \frac{d}{dt} r_i = v_i \quad \ldots\ldots (3.6)$$

$$\dot{v}_i = \frac{d}{dt} v_i = a_i = \frac{F_i}{m_i} \quad \ldots\ldots (3.7)$$

Where m_i is the mass of particle i and F_i is the force acting on particle i. generally acceleration (a) is the function of all particles position and their velocities. So it is time dependent function.

There are several numerical algorithms to solve the 1st order differential equation but velocity verlet is one of the most popular algorithms for MD simulation. The equation of this algorithm can be written as:

$$r(t + \Delta t) = r(t) + \Delta t v(t) + \frac{1}{2}(\Delta t)^2 a(t) + O\left((\Delta t^3)\right) \quad \ldots\ldots (3.8)$$

$$a(t + \Delta t) = a\left(r_1(t + \Delta t)\right), \ldots, r_N(t + \Delta t); v_1(t + \Delta t) \ldots\ldots, v_N(t + \Delta t); t + \Delta t) \quad \ldots\ldots (3.9)$$

$$v(t + \Delta t) = v(t) + \frac{1}{2}\Delta t[a(t) + a(t + \Delta t)] + O\left((\Delta t^3)\right) \quad \ldots\ldots (3.10)$$

In many simple MD simulation problem without external magnetic fields, the particles accelerations doesn't depend on their velocity, so equation (3.9) can be replace by

$$a(t + \Delta t) = a(r_1(t + \Delta t), \ldots\ldots, r_N(t + \Delta t); t + \Delta t) \quad \ldots\ldots (3.11)$$

With the help of Eq. (3.8) we can calculate $r(t + \Delta t)$ at the time t and using equation Eq. (3.11) we can find $a(t + \Delta t)$ finally to find the $v(t + \Delta t)$ use the Eq. (3.10). The implicit character of Eq. (3.10) thus disappear when apply the Eq. (3.11) for the acceleration.

Since calculation part of acceleration is most time consuming process of MD simulation code, its combination of advantageous features make the velocity verlet algorithm of choice for wide range of MD application.

3.1.3 Interatomic potential

Interatomic potential is defined as the interaction between pair of atoms or group of atoms in a liquid phase. If binding takes place between the atoms, potential must be having both the natures i.e. attractive and repulsive. The interatomic potential is a function of lattice spacing (interatomic distance, r). It is the heart of MD simulation. In MD simulation we study million of atoms and there are different type of calculation is needed like- calculation of transport (diffusion, thermal conductivity, viscosity), mechanical quantities (elastic constant, plastic yield), and also the modeling of complex phenomena (shear band localization). Output depends on the quality of interatomic potential. If simple potentials are used, there is less accuracy while for very large simulations, more complicated potential give a better result. So many numbers of potentials are used in simulation process. Some potential is discuss below:

3.1.3.1 Empirical Potentials [49]

It is the combination of intra-molecular and inter-molecular contribution. An intra-molecular potential energy function contains the short-range or bonded portion of the potential while inter-molecular potential energy function contains the long range or non-bonded interactions. Mathematical form of empirical potential is given below:

$$V = V_{\text{short-range}} + V_{\text{long-range}}$$

In the simulation bends, torsions and improper torsions are comes under the short-range portion. According to force field these interactions and parameter are define. Let a system which contains the N atoms, we can divide them into long-range potential in different term like- atoms, pairs, triplets etc. so long-range potentials are:

$$V_{\text{long-range}} = \sum_i v_1(r_i) + \sum_i \sum_{j>i} v_2(r_i, r_j) + \sum_i \sum_{j>i} \sum_{k>j>i} v_3(r_i, r_j, r_k) + \cdots \quad \ldots\ldots\ldots (3.12)$$

$\sum_i \sum_{j>i}$ indicates the summation of all pairs containing i and j which does not double count any pair (ij) and also does not include self interactions. In above Eq. ((3.12) first term is due to an external field acting on the particles in a system. The second term is a pair potential

which depends on the magnitude of the pair separation $r_{ij} = |r_i - r_j|$ and third one is represent the three body interactions and so on.

3.1.3.2 Embedded atom method (EAM)

EAM is a semi-empirical, many atom potential to calculate the total energy of metallic system. Total energy is the summation of separation between an atom and its neighbours. EAM potential is frequently used in MD simulation. If there are N atoms in the system then total energy of the system is given in the following equation [50]:

$$E_{total} = \sum_i F_i(\rho_{h,i}) + \frac{1}{2}\sum_{\substack{i,j \\ i \neq j}} \emptyset_{ij}(R_{ij}) \quad \ldots\ldots\ldots\ldots\ldots\ldots\ldots \quad (3.12)$$

3.1.4 Radial distribution function (RDF)

Radial distribution function gives information about how density varies with respect to reference particle. The symbolic presentation of RDF is g(r). This also gives information about structure features of a system, mainly for liquid and amorphous structures.

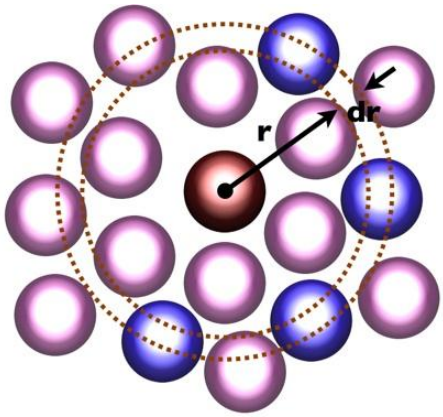

Fig. 3.1: Schematic of radial distribution function

3.1.5 Periodic boundary condition

This boundary condition simulates large system by modelling a small part that is far from its edge. When this boundary condition is used, particle is permitted to cross the box boundaries. When any particle leaves the box at the same instant an identical particle enters the box from neighbours. In MD simulation we assume the periodic boundary conditions particles are affected in their own box and particle in surrounded by box [51]. Fig shows the 2-D representation of periodic boundary condition.

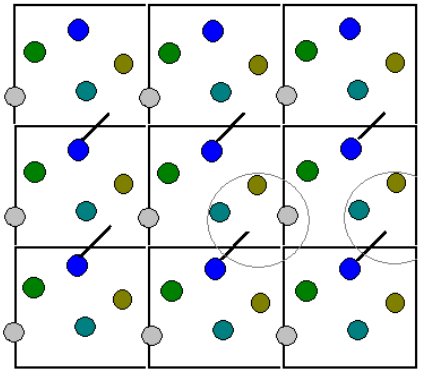

Fig. 3.2: 2-D representation of Periodic Boundary Conditions [52]

3.1.5.1 Limitation of boundary condition

- The size of boxes is larger than the double of cutoff distance (R_{cut}) of the interaction potential.
- The characteristic size of any structural feature in the system of interest or the characteristic length-scale of any important effect should be smaller than the size of the boxes.

3.2 Introduction of LAMMPS (Large-scale Atomic/Molecular Massively Parallel Simulator)

3.2.1 Background and Features

LAMMPS [46] is a powerful MD simulator. It was developed at Sandia National, which is under the United States Department of Energy. This software is free and distributed under the general public licence (GPL). It is operate by codes and the code is easy to modify or extend with new functionality. There are following features of LAMMPS:

- Runs on a single processor or in parallel
- distributed-memory message-passing parallelism (MPI)
- spatial-decomposition of simulation domain for parallelism
- open-source distribution
- optional libraries used: MPI and single-processor FFT
- easy to extend with new features and functionality

- runs from an input script
- syntax for defining and using variables and formulas
- syntax for looping over runs and breaking out of loops
- run one or multiple simulations simultaneously (in parallel) from one script

3.2.2 Ensembles and boundary condition

3.2.2.1 Ensembles

There are different ensembles are used in LAMMPS. These are NPT, NVE, and NVT

3.2.2.2 Boundary condition

There are three boundary conditions involve in LAMMPS. These are:

- p p p
- p p s
- p f p

  Where p stands for periodic along the three directions, 'f' is non-periodic and fix and 's' is non-periodic and shrink wrapped.

3.2.3 Integrators

There are following integrators are used in LAMMPS

- Velocity-Verlet integrator
- Brownian dynamics
- rigid body integration
- energy minimization via conjugate or steepest descent relaxation
- rRESPA hierarchical time stepping

3.3 Visual molecular dynamics (VMD)

VMD is a molecular visualization package for displaying, animating, and analyzing large atoms/molecules using 3-D graphics and built-in scripting. In the present study all the atomic snapshots are taken by VMD software [53].

Chapter 4

Simulation Results & Discussions

4. Simulation results

4.1 Creation of Cu-Zr amorphous alloy

4.1.1 Creation of $Cu_{50}Zr_{50}$ glassy alloy

There are three steps for the formation of $Cu_{50}Zr_{50}$ glassy alloy. In the first step heat the crystalline material up to the temperature of 2300K, after that hold it for 20 ps and then finally quench the model alloy to the room temperature (300 K).

In order to create a glassy model an MD code is written and executed in LAMMPS. The following 'in.file' consists of set of commands that will create a glassy model.

In.file (for size X=50Å, Y=100Å, Z=100Å & cooling rate 10^{14} K/S)

```
 units          metal
echo            both
atom_style      atomic
dimension       3
boundary        p p p
region          box block 0 50 0 100 0 50  units box
create_box      2 box
 lattice        fcc 3.61
 region         cu block 0 50 0 100  0 50 units box
create_atoms    1 region cu units box
# creating composition using set command for Cu50Zr50 alloy
 set            region cu type/fraction 2 0.5 12393
 timestep       0.002
 pair_style     eam/fs
 pair_coeff     * * Cuzr_mm.eam.fs Cu Zr
# Energy Minimization
 minimize       1.0e-3 1.0e-6 1000 10000
 thermo         100
 thermo_style   custom step temp  vol press etotal
 dump           1 all atom 10000 5050_ajn_large.lammpstrj
 dump_modify    1 scale no log log5050_ajn_large.data
 velocity       all create 300.0 873847 rot yes mom yes dist Gaussian
```

Initialization

Out put

```
#fixes
    compute          myRDF all rdf 100
     fix       2  all ave/time 1000 1 1000 c_myRDF file  Cu_zr_quench_large.rdf mode vector
     fix              1 all npt temp 300 2300 0.1 iso 0.0 0.0 0.2
     run              10000
     unfix            1
     fix              1 all npt temp 2300 2300 0.1 iso 0.0 0.0 0.2
     run              20000                                              Heat treatment
     unfix            1
     fix              1 all npt temp 2300 300 0.1 iso 0.0 0.0 0.2
     run              10000
    unfix             1
```

4.1.1.1 Radial distribution function plots (RDF plots)

Fig. 4.1a shows the RDF plot of the $Cu_{50}Zr_{50}$ crystalline model which clearly indicates sharp peaks corresponding to crystalline nature while in Fig. 4.1b shows the RDF plots of the quenched structure which show broad peaks corresponding to amorphous nature.

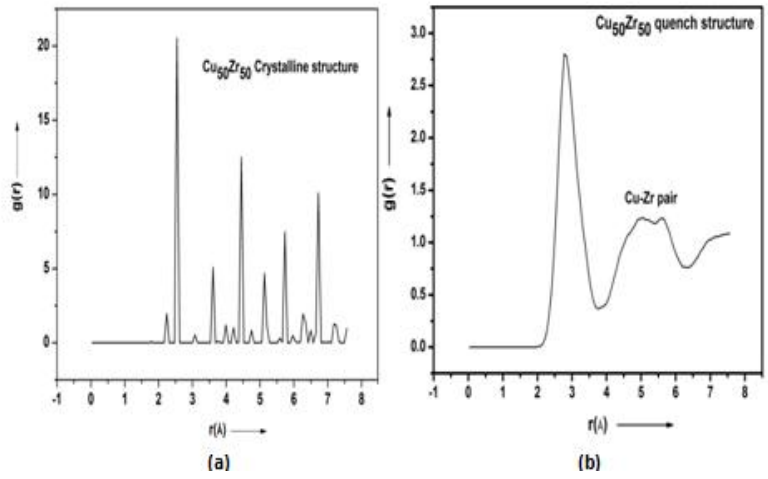

Fig. 4.1: RDF plot for $Cu_{50}Zr_{50}$ (a) crystalline structure (b) glassy structure.

4.1.1.2 VMD snap shots

We can see the difference between crystalline model and glassy model from VMD snaps shots (Fig. 4.2). In crystalline model (Fig. 4.2a) all atoms are arranged in regular manner while that in glassy model (Fig. 4.2b) the atoms are at random positions.

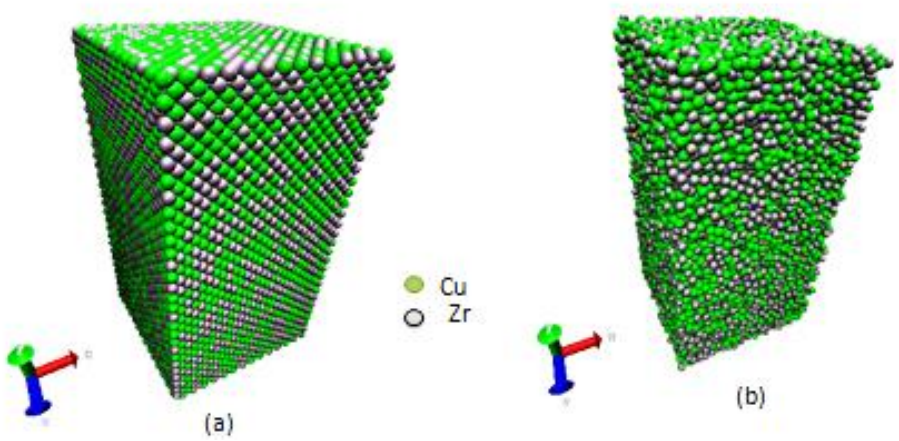

Fig.4.2: VMD snaps shots of $Cu_{50}Zr_{50}$ for (a) crystalline model (b) glassy model of size 50Å×100Å×50Å.

4.1.1.3 Volume- Temperature plot

In Fig. 4.3a shows the volume-temperature plot during heating from 300 K to 2300 K. volume increases with increase in temperature. Fig.4.3b represents volume change with temperature during quenching at cooling rate of 10^{14} K/s. Unlike crystalline materials we do not observe any sharp decrease in volume confirming that the obtained structure is glass.

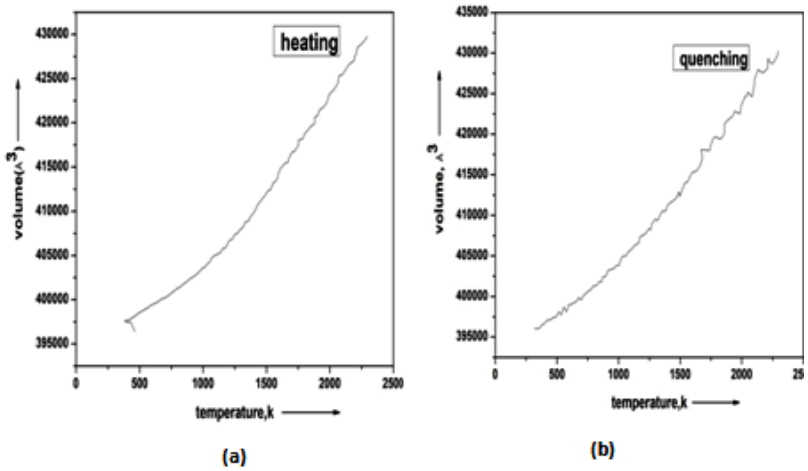

Fig. 4.3: Volume-Temperature plot during (a) heating (b) quenching (10^{14} K/S).

4.1.1.4 Tensile deformation of quenched specimen

After the formation of glassy model, uniaxial tensile deformation has been carried out at two temperatures i.e. 300 K and 500 K and at three different strain rates (1×10^{10} s^{-1}, 2×10^{10} s^{-1} and 4×10^{10} s^{-1}) in order to study the effect of strain rate and temperature. Also the sample was subjected to 40% strain. At the end of the tensile test the mechanical properties

such as Young's modulus, yield strength, and ultimate tensile strength of the glassy alloy were calculated

4.1.1.4.1 Effect of strain rate

Fig. 4.4 shows the stress-strain behavior of $Cu_{50}Zr_{50}$ glassy model at three different strain rates and at 300 K. All the curves show linear elastic region and plastic region. Up to 2% strain the curves show linear elastic behavior which is the characteristic of metallic glasses [54]. With increasing strain rate there is significant increase in the stress. All the curves show flow softening and flow saturation beyond 10% strain.

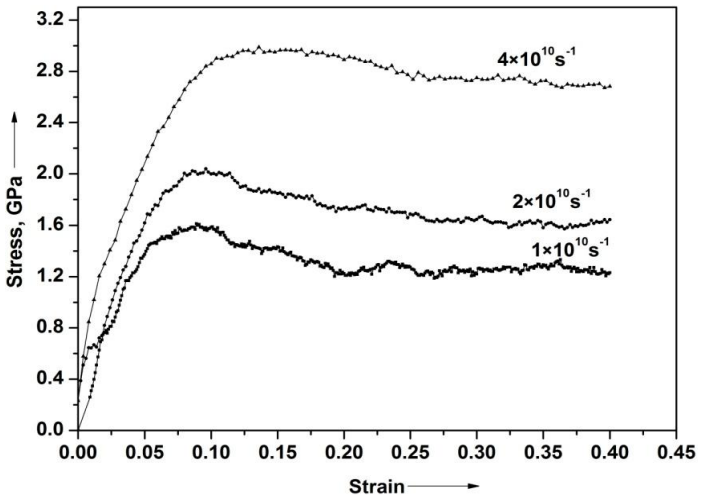

Fig. 4.4: Stress-Strain curve of $Cu_{50}Zr_{50}$ at 300K for three different strain rates ($1 \times 10^{10}\ s^{-1}$, $2 \times 10^{10}\ s^{-1}$ and $4 \times 10^{10}\ s^{-1}$).

The mechanical properties of the alloy at different strain rates are tabulated in Table 4.1. From the Table 4.1 we can see that the ultimate tensile stress varies from 1.63 GPa to 3.01 GPa, yield stress varies from 0.54 GPa to 1.40 GPa and Young's modulus varies from 68.3 GPa to 98.4 GPa with increasing strain rate. In the studies of [6] modulus values obtained were in the range of 63-83 GPa.

Table 4.1: Mechanical properties of $Cu_{50}Zr_{50}$ glass at three different strain rates

Alloy Composition	Temperature (in Kelvin)	Strain rate (S^{-1})	Yield stress (in GPa)	UTS (in GPa)	Young's Modulus(GPa)
		1×10^{10}	0.54	1.38	65.3
$Cu_{50}Zr_{50}$	300K	2×10^{10}	0.65	2.04	84.3
		4×10^{10}	1.40	3.01	98.4

4.1.1.4.2 Effect of temperature

Fig. 4.5 shows the stress-strain behavior at 300 K and 500 K at strain rate of 2×10^{10} s^{-1}. The curves show linear elastic region and plastic region. With increasing strain beyond 10% flow softening and flow saturation is observed. The flow curve of the sample deformed at 500 K is significantly lower than that of the sample deformed at 300 K which could be due to the rapid diffusion of free volume at high temperature.

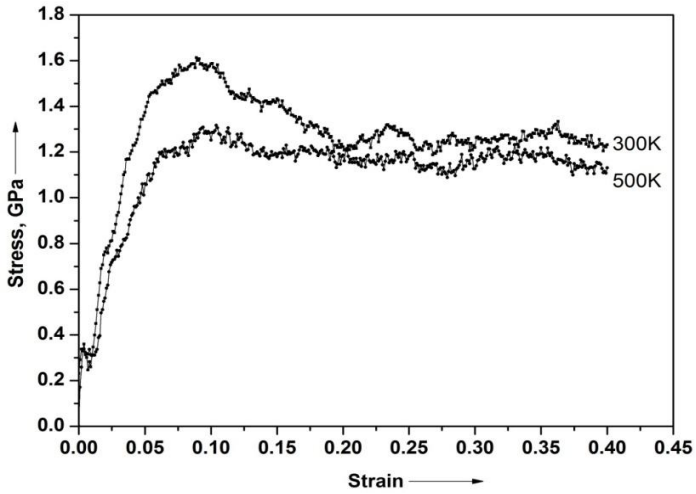

Fig. 4.5: Stress-Strain curve of $Cu_{50}Zr_{50}$ at temperatures 300K and 500K

4.2 Creation of Cu-Zr-Al glassy alloys

4.2.1 Creation of $Cu_{49}Zr_{49}Al_2$ alloy

There are three steps for the formation of $Cu_{49}Zr_{49}Al_2$ glassy alloy. In first step heat the crystalline material up to the temperature of 2300K followed by holding for 20 ps and then finally quenching the model to the room temperature (300 K).

In order to create a glassy model an MD code is written and executed in LAMMPS. The following 'in.file' consists of set of commands that will create a glassy model.

 # In.file (for size X=50Å, Y=100Å, Z=100Å & cooling rate 10^{14} K/S)

```
units          metal
echo           both
atom_style     atomic
dimension      3
```

```
boundary        p p p
region          box block 0 50 0 100 0 50  units box
create_box      3 box
lattice         fcc 3.61
region          cu block 0 50 0 100  0 50 units box
create_atoms    1 region cu units box
# creating composition by using set command for cuzral alloy
set             region cu type/fraction 2 0.49 12393
set             region cu type/fraction 3 0.02 12393
timestep        0.002
pair_style      eam/alloy
pair_coeff      * * CuZrAl.set Cu Zr Al
# Energy Minimization
minimize        1.0e-4 1.0e-6 10000 100000
thermo          100
thermo_style    custom step temp  vol press etotal
dump            1 all atom 10000 ternary_cuzral.dump.lammpstrj
dump_modify     1 scale no
log logcuzral2.data
compute         myRDF all rdf 1000
fix             11 all ave/time 1000 1 1000 c_myRDF file
 cuzral2.rdf mode vector
velocity        all create 300.0 873847 rot yes mom yes dist gaussian
fix             1 all npt temp 300 2300 0.2 iso 0.0 0.0 0.2
run             10000
unfix           1
fix             1 all npt temp 2300 2300 0.2 iso 0.0 0.0 0.2
run             20000
unfix           1
fix             1 all npt temp 2300 300  0.2 iso 0.0 0.0 0.2
run             10000
unfix           1
```

4.2.1.1 Radial distribution function plots (RDF plots)

Fig. 4.6a shows the RDF plot of the $Cu_{49}Zr_{49}Al_2$ crystalline model which clearly indicates sharp peaks corresponding to crystalline nature while in Fig. 4.6b shows the RDF plots of the quenched structure which show broad peaks corresponding to amorphous nature.

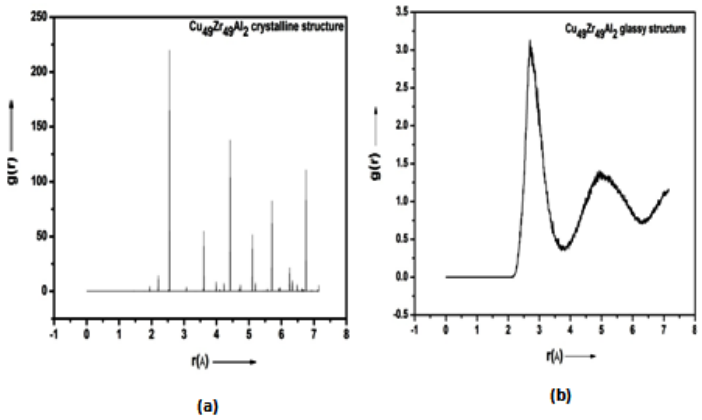

Fig. 4.6: RDF plot for $Cu_{49}Zr_{49}Al_2$ (a) crystalline structure (b) glassy structure

4.2.1.2 VMD snap shots

We can see the difference between crystalline model and glassy model from VMD snaps shots (Fig. 4.7). In crystalline model (Fig. 4.7a) all atoms are arranged in regular manner while that in glassy model (Fig. 4.7b) the atoms are randomly placed.

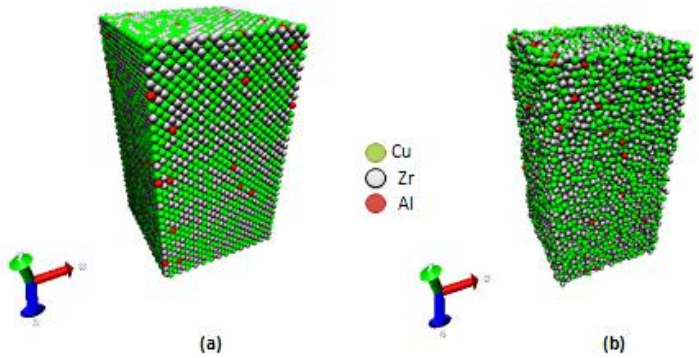

Fig.4.7: VMD snaps shots of $Cu_{49}Zr_{49}Al_2$ for (a) crystalline model (b) glassy model of size 50Å×100Å×50Å.

4.2.1.3 Volume- Temperature plot

In Fig. 4.8a shows the volume-temperature plot during heating from 300 K to 2300 K. volume increases with increase in temperature. Fig.4.8b represents volume change with temperature during quenching at cooling rate of 10^{14} K/s. Unlike crystalline materials we do not observe any sharp decrease in volume confirming that the obtained structure is glass.

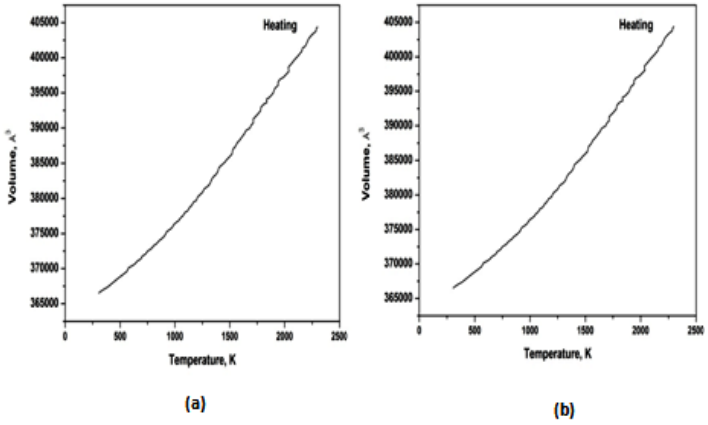

Fig. 4.8: Volume-Temperature plot for $Cu_{49}Zr_{49}Al_2$ during (a) heating (b) quenching (10^{14} K/S).

4.2.1.4 Tensile deformation of quenched specimen

In order to perform a tensile test MD code is written and executed in LAMMPS. The following 'in.file' consists of set of commands that will perform tensile test.

In.file

```
units           metal
boundary        p p p
atom_style      atomic
echo            both
read_data       cu49zr49al2.txt
timestep        0.001

pair_style      eam/alloy
pair_coeff      * * CuZrAl.set Cu Zr Al

# Energy Minimization
# minimize      1.0e-5 1.0e-10 10000 100000
```

```
dump            1 all atom 10000 dump.2al_300k_test.lammpstrj
log log2al_300k_test.dat
# initial velocities
velocity        all create 298 482748 rot yes mom yes dist gaussian
fix             1 all deform 1 y erate 0.01
fix             2 all npt temp 300.0 300.0 10.0 x 0 0 10.0 z 0 0 10.0   dilate all
fix             3 all temp/rescale 10 300 300 0.05 1.0
compute         11 all rdf 100
fix             4 all ave/time 100 1 100 c_11 file rdf_2al_300k_test.rdf mode vector
compute         1 all stress/atom
compute         2 all temp
dump            2 all custom 10000 dump.stress_atom_2al-300k_test type x y z c_1[1]
                c_1[2] c_1[3] c_1[4] c_1[5] c_1[6]
compute         3 all reduce sum c_1[2]
variable        stress equal c_3/(3*250000)
variable        stress_GPa equal v_stress/10000
thermo          100
thermo_style    custom step temp press vol etotal c_2 v_stress v_stress_GPa
run             40000
```

Uniaxial tensile deformation

4.2.1.4.1 Effect of strain rate

Fig. 4.9 shows the stress-strain behavior of $Cu_{49}Zr_{49}Al_2$ glassy model at three different strain rates and at 300 K. All the curves show linear elastic region and plastic region. Up to 2% strain the curves show linear elastic behavior which is the characteristic of metallic glasses [54]. With increasing strain rate there is significant increase in the stress. All the curves show flow softening and flow saturation beyond 7.5% strain.

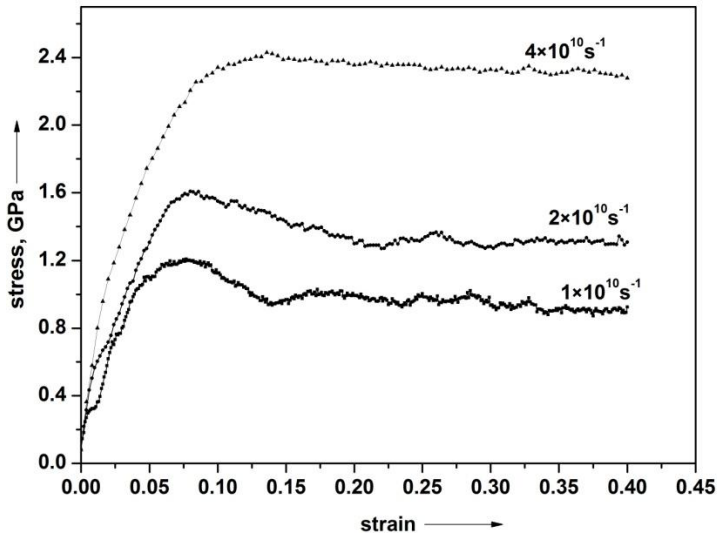

Fig. 4.9: Stress-Strain curve of $Cu_{49}Zr_{49}Al_2$ alloy at 300K for three different strain rates (1×10^{10} s^{-1}, 2×10^{10} s^{-1} and 3×10^{10} s^{-1})

The mechanical properties of the alloy at different strain rates are tabulated in Table 4.2. From the Table 4.2 we can see that the yield stress varies from 0.57 GPa to 1.45 GPa, ultimate tensile stress varies from 1.40 GPa to 2.43 GPa and Young's modulus varies from 70.01 GPa to 101.3 GPa with increasing strain rate. As per Ref. 13 modulus values obtained were in the range of 79-94 GPa.

Table 4.2: Mechanical properties of $Cu_{49}Zr_{49}Al_2$ glass at three different strain rates.

Alloy Composition	Temperature (in Kelvin)	Strain rate (s^{-1})	Yield stress (in GPa)	UTS (in GPa)	Young's Modulus(GPa)
		1×10^{10}	0.572	1.40	70.01
$Cu_{49}Zr_{49}Al_2$	300K	2×10^{10}	0.661	1.60	87.25
		4×10^{10}	1.454	2.43	101.3

4.2.1.4.2 Effect of temperature

Fig. 4.6 shows the effect of temperature on the stress-strain behavior at 300 K and 500 K and at strain rate of 1×10^{10} s^{-1}. The curves show linear elastic region and plastic region. With increasing strain beyond 10% flow softening and flow saturation is observed. The alloy deformed at 300 K shows maximum stress of 1.2 GPa while that the deformed at 500 K shows maximum stress of 1.1 GPa.

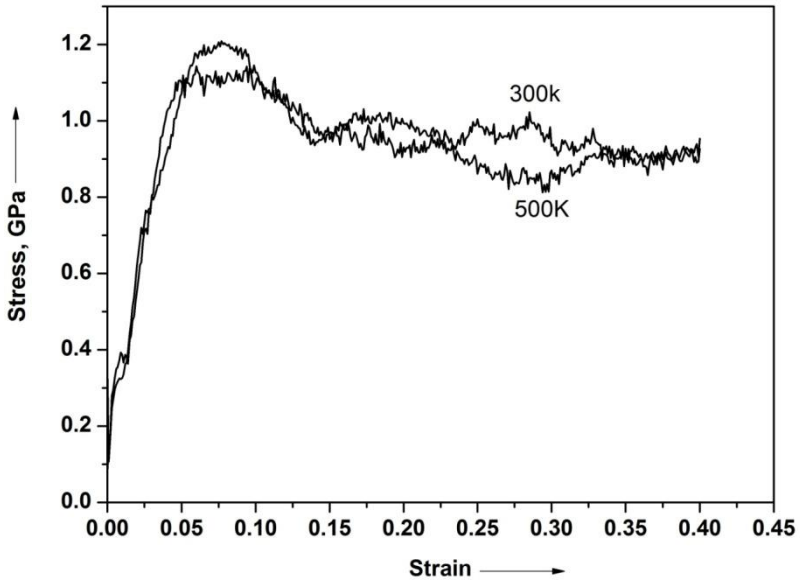

Fig. 4.10: Stress-Strain curve of $Cu_{49}Zr_{49}Al_2$ at temperatures 300 K and 500 K at 0.01 ps^{-1}

4.2.2 Creation of $Cu_{45}Zr_{45}Al_{10}$ alloy

4.2.2.1 Radial distribution function plots (RDF plots)

Fig. 4.11a shows the RDF plot of the $Cu_{45}Zr_{45}Al_{10}$ crystalline model which clearly indicates sharp peaks corresponding to crystalline nature while in Fig. 4.11b shows the RDF plots of the quenched structure which show broad peaks corresponding to amorphous nature.

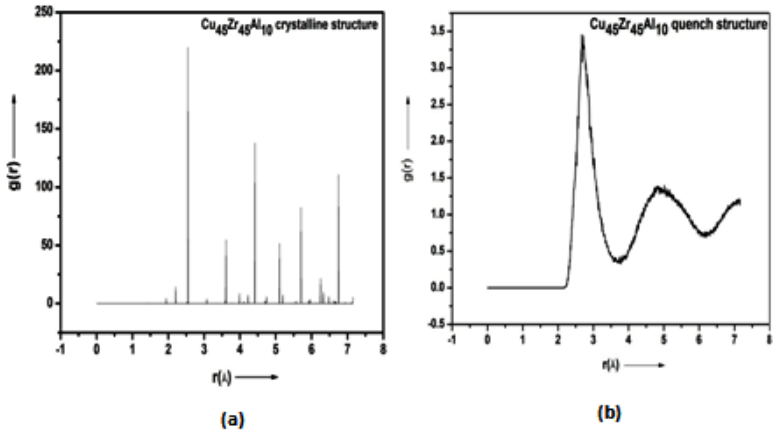

Fig. 4.11: RDF plot for $Cu_{45}Zr_{45}Al_{10}$ (a) crystalline structure (b) glassy structure.

4.2.2.2 VMD snap shots

We can see the difference between crystalline model and glassy model from VMD snaps shots (Fig. 4.12). In crystalline model (Fig. 4.12a) all atoms are arranged in regular manner while that in glassy model (Fig. 4.12b) the atoms are randomly placed.

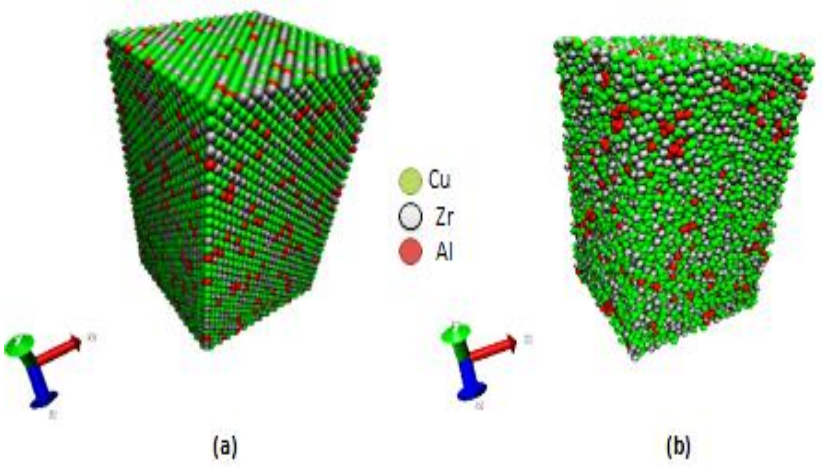

Fig.4.12: VMD snaps shots of $Cu_{45}Zr_{45}Al_{10}$ for (a) crystalline model (b) glassy model of size 50Å×100Å×50Å.

4.2.2.3 Volume- Temperature plot

In Fig. 4.13a shows the volume-temperature plot during heating from 300 K to 2300 K. Volume increases with increase in temperature. Fig.4.13b represents volume change with temperature during quenching at cooling rate of 10^{14} K/s. Unlike crystalline materials we do not observe any sharp decrease in volume confirming that the obtained structure is glass.

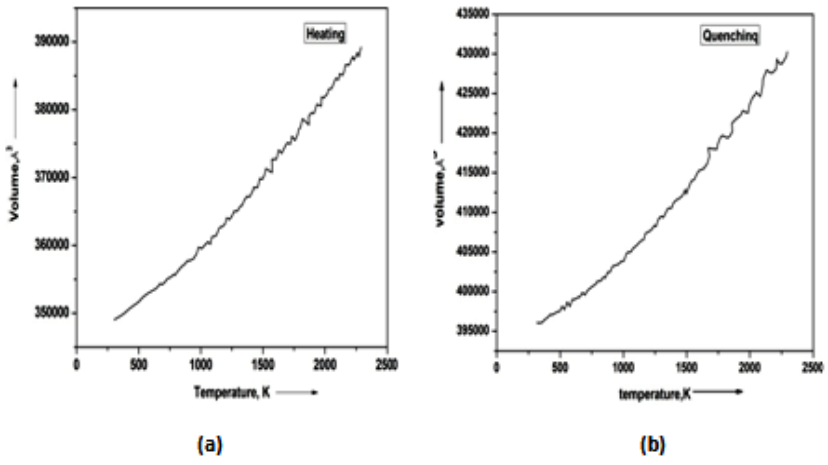

Fig. 4.13: Volume-Temperature plot for $Cu_{45}Zr_{45}Al_{10}$ during (a) heating (b) quenching (10^{14} K/s).

4.2.2.4 Tensile deformation of quenched specimen

4.2.2.4.1 Effect of strain rate

Fig. 4.14 shows the stress-strain behavior of $Cu_{45}Zr_{45}Al_{10}$ glassy model at three different strain rates and at 300 K. All the curves show linear elastic region and plastic region. Up to 2% strain the curves show linear elastic behavior which is the characteristic of metallic glasses [54]. With increasing strain rate there is significant increase in the stress. All the curves show flow softening and flow saturation beyond 7.5% strain.

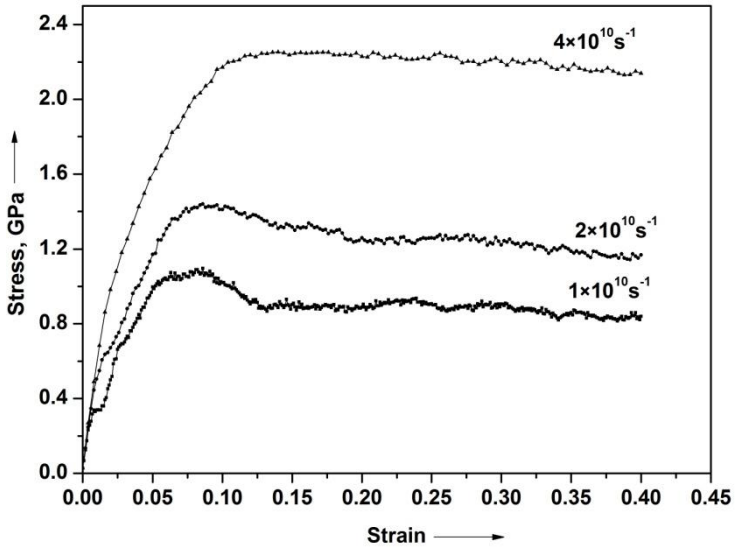

Fig. 4.14: Stress-Strain curve of $Cu_{45}Zr_{45}Al_{10}$ alloy at 300K for three different strain rates ($1 \times 10^{10}\ s^{-1}$, $2 \times 10^{10}\ s^{-1}$ and $3 \times 10^{10}\ s^{-1}$)

The mechanical properties of the alloy at different strain rates are tabulated in Table 4.3. From the Table 4.3 we can see that the yield stress varies from 0.59 GPa to 1.52 GPa, ultimate tensile stress varies from 1.09 GPa to 2.27 GPa and Young's modulus varies from 83.3 to 94.6 GPa GPa with increasing strain rate. As per Ref. 13 modulus values obtained are in the range of 83-94 GPa.

Table 4.3: Mechanical properties of $Cu_{45}Zr_{45}Al_{10}$ glass at three different strain rates.

Alloy Composition	Temperature (in Kelvin)	Strain rate (s^{-1})	Yield stress (in GPa)	UTS (in GPa)	Young's Modulus(GPa)
		1×10^{10}	0.59	1.09	83.3
$Cu_{45}Zr_{45}Al_{10}$	300K	2×10^{10}	0.69	1.44	88.9
		4×10^{10}	1.52	2.27	94.6

4.2.2.4.2 Effect of temperature

Fig. 4.15 shows the effect of temperature on the stress-strain behavior at 300 K and 500 K at strain rate of 1×10^{10} s^{-1}. The curves show linear elastic region and plastic region. With increasing strain beyond 7.5% flow softening and flow saturation is observed. Further, there was no significant difference in the stress-strain behavior.

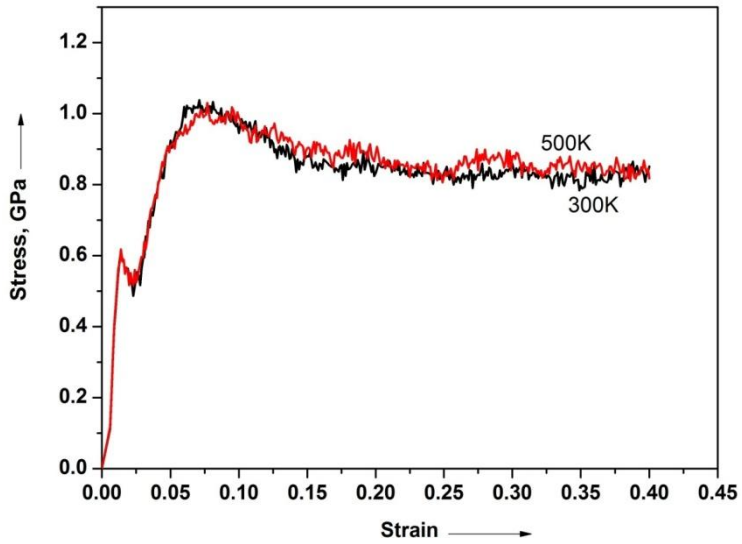

Fig. 4.15: Stress-Strain curve of $Cu_{45}Zr_{45}Al_{10}$ alloy at two different temperatures (300K and 500K) at 0.01 ps^{-1}

4.3 Creation of Cu-Zr-Ti glassy alloys

4.3.1 Creation of $Cu_{50}Zr_{48}Ti_2$ glassy alloy

4.3.1.1 RDF plots

Fig. 4.16a shows the RDF plot of the $Cu_{50}Zr_{48}Ti_2$ crystalline model which clearly indicates sharp peaks corresponding to crystalline nature while in Fig. 4.16b shows the RDF plots of the quenched structure which show broad peaks corresponding to amorphous nature.

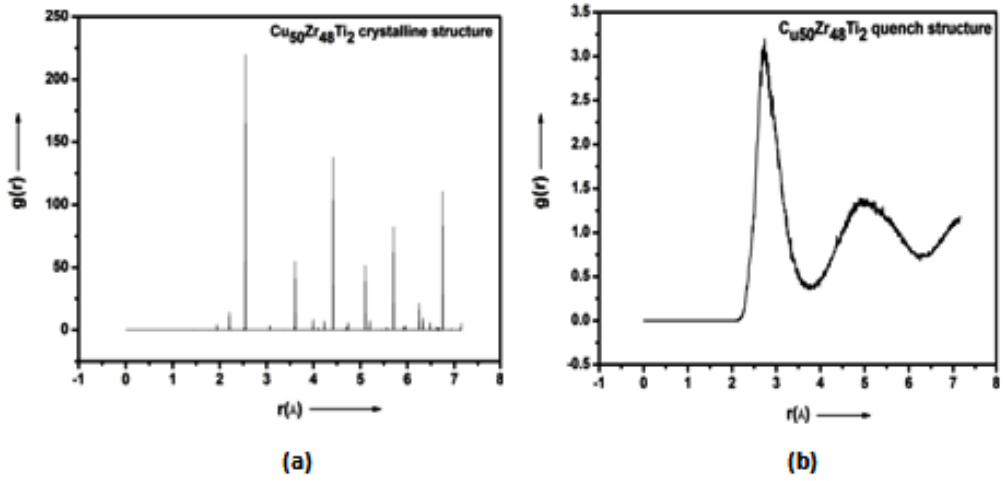

Fig. 4.16: RDF plot for $Cu_{50}Zr_{48}Ti_2$ (a) crystalline structure (b) glassy structure

4.3.1.2 VMD snaps shots

We can see the difference between crystalline model and glassy model from VMD snaps shots (Fig. 4.17). In crystalline model (Fig. 4.17a) all atoms are arranged in regular manner while that in glassy model (Fig. 4.17b) the atoms are randomly placed.

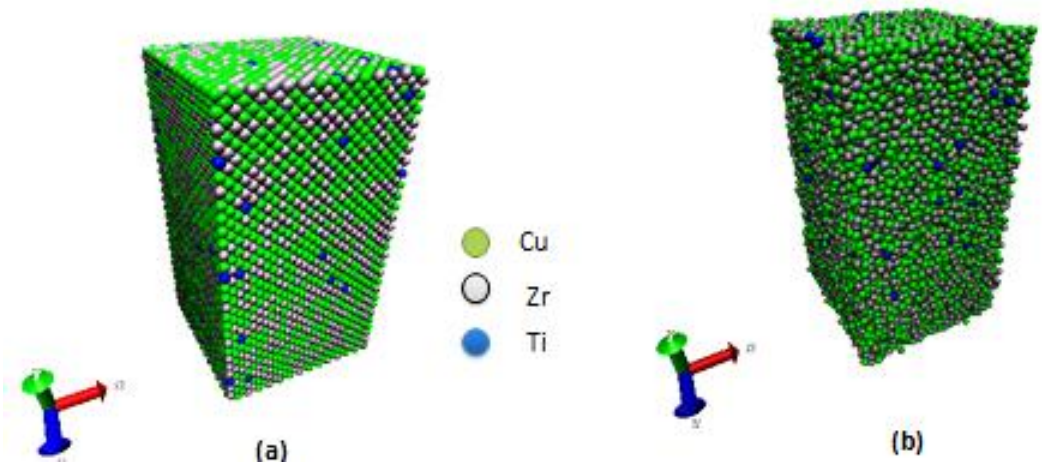

Fig.4.17: VMD snaps shots of $Cu_{50}Zr_{48}Ti_2$ for (a) crystalline model (b) glassy model of size 50Å×100Å×50Å.

4.3.1.3 Volume- Temperature plot

In Fig. 4.18a shows the volume-temperature plot during heating from 300 K to 2300 K. volume increases with increase in temperature. Fig.4.18b represents volume change with temperature during quenching at cooling rate of 10^{14} K/s. Unlike

crystalline materials we do not observe any sharp decrease in volume confirming that the obtained structure is glass.

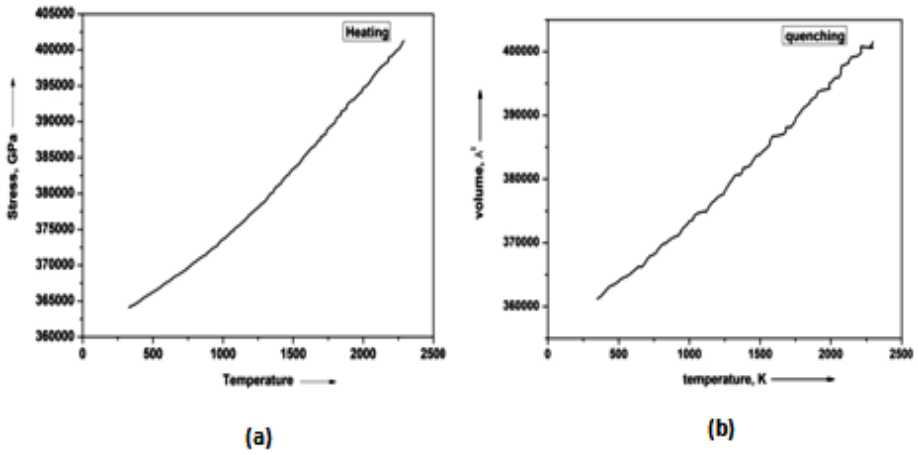

Fig. 4.18: Volume-Temperature plot for $Cu_{50}Zr_{48}Ti_2$ during (a) heating (b) quenching (10^{14} K/s)

4.3.1.4 Tensile deformation of quenched specimen

4.3.1.4.1 Effect of strain rate

Fig. 4.19 shows the room temperature stress-strain behavior of $Cu_{50}Zr_{48}Ti_2$ glassy at three different strain rates. All the curves show linear elastic region and plastic region. Up to 2% strain the curves show linear elastic behavior which is the characteristic of metallic glasses [51]. With increasing strain rate there is significant increase in the stress. The curves deformed at strain rate of 1×10^{10} s^{-1} and 2×10^{10} s^{-1} show flow softening and flow saturation beyond 7.5% strain while that deformed at strain rate of 4×10^{10} s^{-1} show strain hardening behavior.

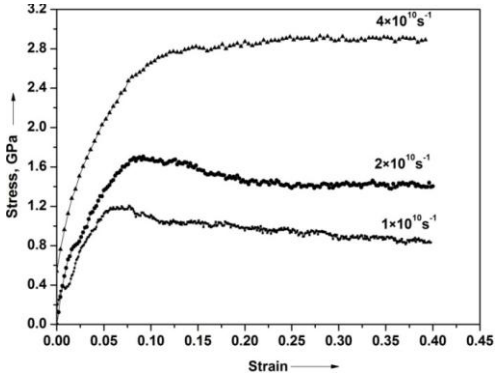

Fig. 4.19: Stress-Strain curve of $Cu_{50}Zr_{48}Ti_2$ alloy at 300 K for three different strain rates (1×10^{10} s^{-1}, 2×10^{10} s^{-1} and 3×10^{10} s^{-1})

Table 4.4: Mechanical properties of $Cu_{50}Zr_{44}Ti_6$ glass at three different strain rates.

Alloy Composition	Temperature (in Kelvin)	Strain rate (S^{-1})	Yield stress (in GPa)	UTS (in GPa)	Young's Modulus(GPa)
		1×10^{10}	0.68	1.21	70.2
$Cu_{50}Zr_{48}Ti_2$	300 K	2×10^{10}	1.10	1.72	77.3
		4×10^{10}	1.20	2.94	82.8

The mechanical properties of the alloy at different strain rates are tabulated in Table 4.4. From the Table 4.4 we can see that the yield stress varies from 0.68 GPa to 1.20 GPa, ultimate tensile stress varies from 1.21 GPa to 2.94 GPa and Young's modulus varies from 70.2 GPa to 82.8 GPa with increasing strain rate. Literature reports modulus values in the range of 71- 83 GPa in Cu-Zr-Ti metallic glasses [40].

4.3.1.4.2 Effect of temperature

Fig. 4.20 shows the effect of temperature on the stress-strain behavior at 300 K and 500 K at strain rate of 1×10^{10} s^{-1}. The curves show linear elastic region and plastic region. With increasing strain beyond 7.5% flow softening and flow saturation is observed. The maximum stress at 500 K is much higher than that at 300 K which is unusual.

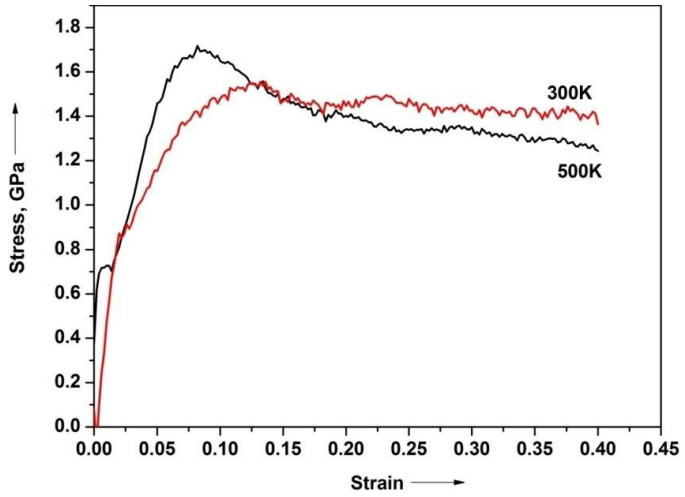

Fig. 4.20: Stress-Strain curve of $Cu_{50}Zr_{48}Ti_2$ alloy at two different temperatures (300 K and 500 K) at 2×10^{10} s^{-1}

4.3.2 Creation of $Cu_{50}Zr_{44}Ti_6$ glassy alloy

4.3.2.1 RDF plots

Fig. 4.21a shows the RDF plot of the $Cu_{50}Zr_{44}Ti_6$ crystalline model which clearly indicates sharp peaks corresponding to crystalline nature while in Fig. 4.21b shows the RDF plots of the quenched structure which show broad peaks corresponding to amorphous nature.

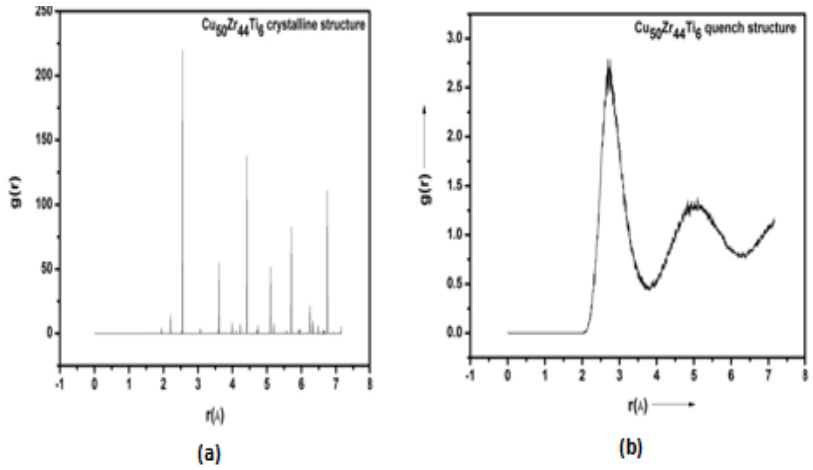

Fig. 4.21: RDF plot for $Cu_{50}Zr_{44}Ti_6$ (a) crystalline structure (b) glassy structure.

4.3.2.2 VMD snaps shots

We can see the difference between crystalline model and glassy model from VMD snaps shots (Fig. 4.22). In crystalline model (Fig. 4.22a) all atoms are arranged in regular manner while that in glassy model (Fig. 4.22b) the atoms are randomly placed.

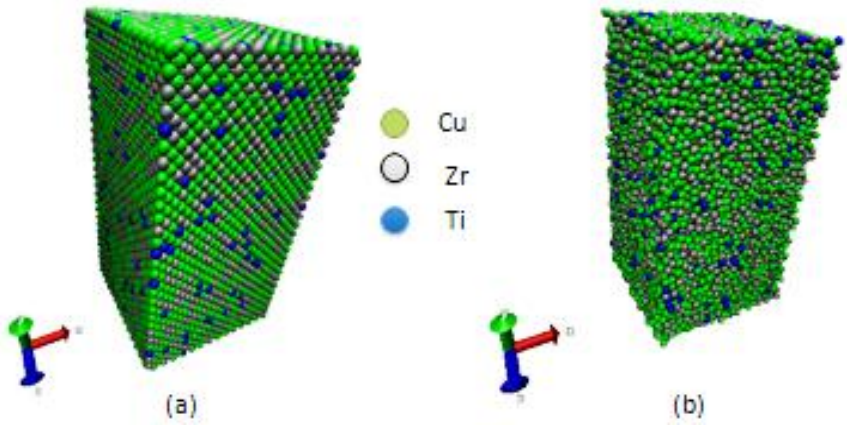

Fig.4.22: VMD snaps shots of $Cu_{50}Zr_{44}Ti_6$ for (a) crystalline model (b) glassy model of size 50Å×100Å×50Å.

4.3.2.3 Volume - Temperature plot

In Fig. 4.23a shows the volume-temperature plot during heating from 300 K to 2300 K. volume increases with increase in temperature. Fig.4.23b represents volume change with temperature during quenching at cooling rate of 10^{14} K/s. Unlike crystalline materials we do not observe any sharp decrease in volume confirming that the obtained structure is glass.

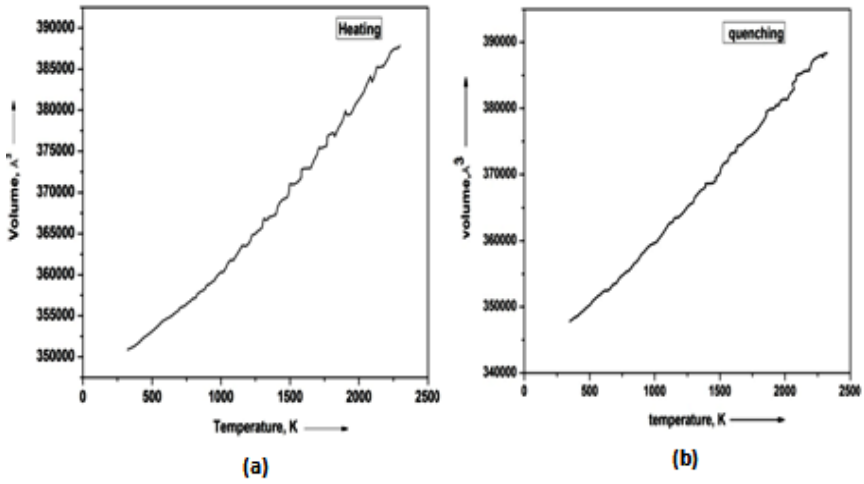

Fig. 4.23: Volume-Temperature plot for $Cu_{50}Zr_{44}Ti_6$ during (a) heating (b) quenching at 10^{14} K/s.

4.3.2.4 Tensile deformation of quenched specimen

4.3.2.4.1 Effect of strain rate

Fig. 4.24 shows the stress-strain behavior of $Cu_{50}Zr_{48}Ti_6$ glassy model at three different strain rates and at 300 K. All the curves show linear elastic region and plastic region. Up to 2% strain the curves show linear elastic behavior which is the characteristic of metallic glasses [51]. With increasing strain rate there is significant increase in the stress. All the curves show flow softening and flow saturation beyond 7.5% strain.

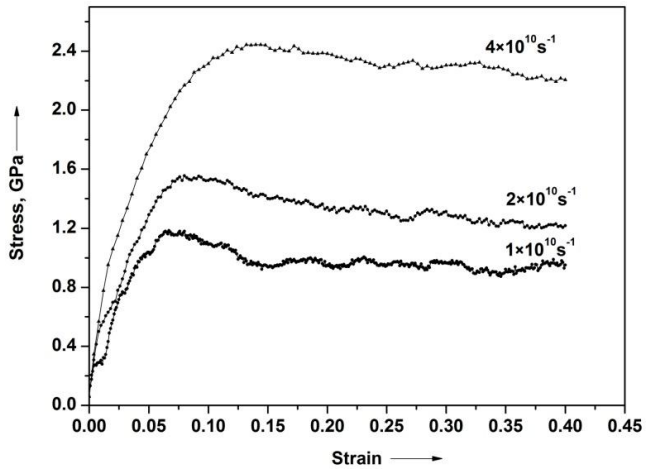

Fig. 4.24: Stress-Strain curve of $Cu_{50}Zr_{44}Ti_6$ alloy at 300K for three different strain rates (1×10^{10} s^{-1}, 2×10^{10} s^{-1} and 3×10^{10} s^{-1}).

The mechanical properties of the alloy at different strain rates are tabulated in Table 4.5. From the Table 4.5 we can see that the yield stress varies from 0.45 GPa to 2.26 GPa, ultimate tensile stress varies from 1.19 GPa to 2.46 GPa and Young's modulus varies from 71.3 GPa to 84.6 GPa with increasing strain rate. In the studies of [40] modulus values obtained were in the range of 71- 83 GPa.

Table 4.5: Mechanical properties of $Cu_{50}Zr_{44}Ti_6$ glass at three different strain rates.

Alloy Composition	Temperature (in Kelvin)	Strain rate (s^{-1})	Yield stress (in GPa)	UTS (in GPa)	Young's Modulus(GPa)
		1×10^{10}	0.45	1.19	71.3
$Cu_{50}Zr_{44}Ti_6$	300K	2×10^{10}	0.75	1.56	79.5
		4×10^{10}	2.26	2.46	84.6

4.3.2.4.2 Effect of temperature

Fig. 4.25 shows the effect of temperature on the stress-strain behavior at 300 K and 500 K at strain rate of 1×10^{10} s^{-1}. The curves show linear elastic region and plastic region. With increasing strain beyond 7.5% flow softening and flow saturation is observed. The flow stress is higher at 300 K and the curves superimpose after 15% strain.

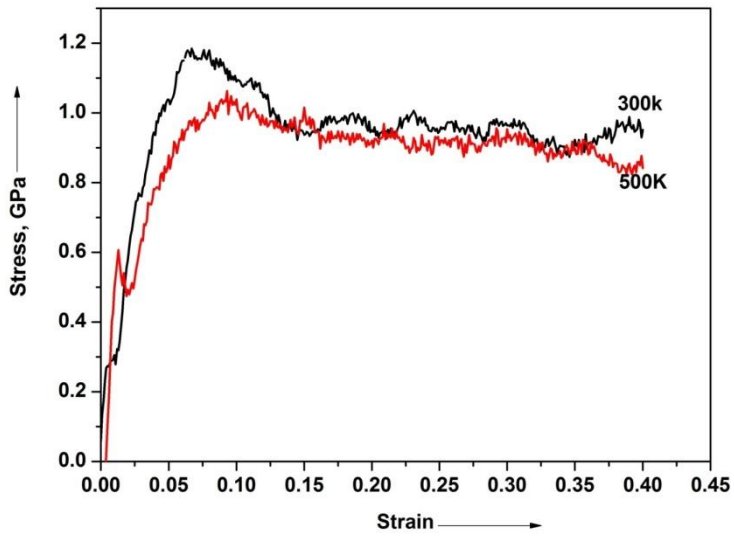

Fig. 4.25: Stress-Strain curve of $Cu_{50}Zr_{44}Ti_6$ alloy at two different temperatures (300K and 500 K) at 0.01 PS^{-1}

****

4.4 Discussions

4.4.1 Effect of composition

Simulation of high strain rate plastic deformation, which is known to occur by shearing of STZ, also suggests that Al addition reduces the flow stress considerably. In Fig. 4.26 Cu-Zr-Al alloy which contain less amount of Al (2 at. %.) has high flow stresses compared to that which contain high amount of Al (10 at. %). Similarly addition of Ti also reduces the flow stress considerably.

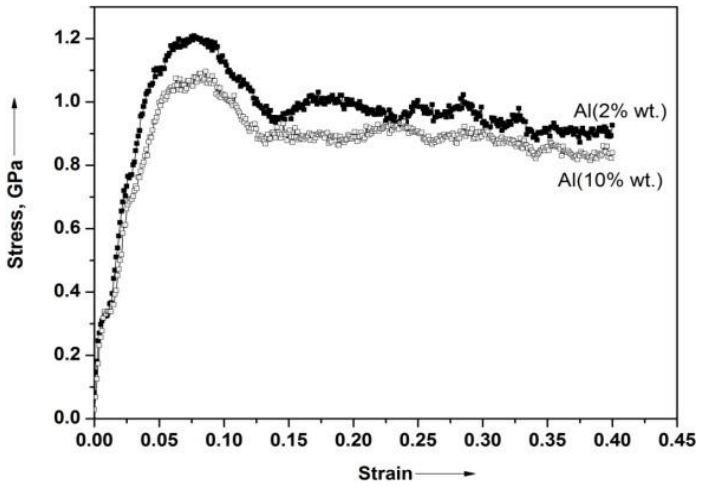

Fig. 2.26: Stress-Strain curve of Cu-Zr-Al alloys for different composition of Al at strain rate of 1×10^{10} s^{-1}

4.4.2 Effect of temperature

In most of the alloys the flow curve of the sample deformed at 500 K is significantly lower than that of the sample deformed at 300 K which could be due to the rapid diffusion of free volume at high temperature.

4.4.3 Effect of strain rate

As the strain rate is increased from $1 \times 10^{10}s^{-1}$ to $4 \times 10^{10}s^{-1}$, the flow stress is expected to increase. This is valid for diffusive mechanism as well as STZ mechanism. Curves show flow softening and flow saturation beyond 7.5% strain.

Chapter 5
Conclusions

5 Conclusions:

(a) Addition of Al to Cu-Zr alloys has lowered the flow stress and ultimate tensile stress, increased the Young's modulus.

(b) Addition of Ti to Cu-Zr alloy also decreased the yield stress.

(c) MD simulations showed that with increase in strain rate flow stress increased in the strain rate range of 1×10^{10} s^{-1} – 4×10^{10} s^{-1}.

(d) With increasing the temperature flows stress is lowered due to rapid diffusion of free volume at high temperature.

Chapter 6

References

References:

[1] P. Duwez, F. H. Brown Jun. and F. Odell, the Zirconia -Yttria System, J. Electrochem. Soc. 1951, 98: 356

[2] David lee Henann, Aspect of the mechanics of the metallic glasses, Ph.D thesis, B.S, State University of New York (2006).

[3] H. S. Chen, Metallic Glasses, Chinese Journal of Physics. 1990, 28.

[4] Joysurya Basu and S Ranganathan, Bulk metallic glasses: A new class of engineering materials, Sadhana. 2003, 28: 4783–798.

[5] A. Inoue, W. Zhang, T. Zhang, and K. Kurosaka, High-Strength Cu-based Bulk Glassy Alloys in Cu–Zr–Ti and Cu–Hf–Ti Ternary Systems, Acta mater. 2001, 49: 2645–2652.

[6] Mattern, N., Bednarcik, J., Pauly, S., Wang, G., Das, J., Eckert, Structural evolution of Cu-Zr metallic glasses under tension, Acta Materialia. J. 2009, 57: 4133-4139.

[7] Lee, S. W., Huh, M. Y., Fleury, E., Lee, Crystallization-induced plasticity of Cu-Zr containing bulk amorphous alloys, Acta Materialia. 2006, 54: 349-355.

[8] Wei, X. F., Sun, Y. F., Guan, S. K., Terada, D., Shek, Compressive and tensile properties of CuZrAl alloy plates containing martensitic phases, Materials Science and Engineering. 2009, 517: 375-380.

[9] Xue, Y. F., Cai, H. N., Wang, L., Wang, F. C., Zhang, Effect of loading rate on failure in Zr-based bulk metallic glass, Materials Science and Engineering A. 2008, 473: 105-110.

[10] Mondal, K., Ohkubo, T., Toyama, T., Nagai, Y., Hasegawa, M., Hono, The effect of nanocrystallization and free volume on the room temperature plasticity of Zr-based bulk metallic glasses, Acta Materialia. 2008, 56: 5329-5339.

[11] Pauly, S., Das, J., Duhamel, C., Eckert, Effect of Titanium on Microstructure and Mechanical Properties of $Cu_{50}Zr_{50-x}Ti_x$ ($2.5 \leq x \leq 7.5$) Glass Matrix Composites, Metallurgical and Materials Transactions. 2008, 39: 1868-1873.

[12] Das, J., Tang, M. B., Kim, K. B., Theissmann, R., Baier, F., Wang, W. H., Eckert, "Work-Hardenable" Ductile Bulk Metallic Glass, Physical Review Letters. 2005, 94: 2055.

[13] Pauly, S., Liu, G., Wang, G., Kühn, U., Mattern, N., Eckert, Microstructural heterogeneities governing the deformation of $Cu_{47.5}Zr_{47.5}Al_5$ bulk metallic glass composites, Acta Materialia. 2009, 57: 5445-5453.

[14] Hajime Tanaka, Relationship among glass-forming ability, fragility, and short-range bond ordering of liquids, Journal of Non-Crystalline Solids. 2005, 351: 678–690.

[15] MEI Jinna, Titanium-based Bulk Metallic Glasses: Glass Forming Ability and Mechanical Behavior, PhD Thesis, Joseph Fourier University – Grenoble Northwestern Polytechnical University.

[16] Debenedetti, P. G., Stillinger, F. H., Truskett, T. M. & Lewis, C. P. Theory of supercooled liquids and glasses: energy landscape and statistical geometry perspectives. Adv. Chem. Eng. (in the press).

[17] Debenedetti, P. G. Metastable Liquids. Concepts and Principles, Princeton Univ. Press, Princeton, 1996.

[18] Turnbull, D. Under what conditions can a glass be formed? Contemp. Phys. 1969, 10: 473–488.

[19] Angell, C. A. Structural instability and relaxation in liquid and glassy phases near the fragile liquid limit, J. Non-Cryst. Solids 102: 205–221.

[20] Moynihan, The Glass Transition and the Nature of the Glassy State, Ann. NY Acad. Sci. 1976, 279: 15–36.

[21] Brüning, R. & Samwer, Glass transition on long time scales, Phys. Rev. 1992, 46: 318–322.

[22] H S Chen, Glassy metals, Rep. Prog. Phys. 1980, 43.

[23] Christopher A. Schuh, Todd C. Hufnagel b, Upadrasta Ramamurty, Mechanical behavior of amorphous alloys, Acta Materialia. 2007, 55: 4067–4109.

[24] Trexler, Thadhani, Mechanical properties of bulk metallic glasses, Prog Mater Sci. 2010, 55: 759-836.

[25] Takeuchi, Maeda K. Microscopic mechanism of plastic deformation in metallic glasses, In: Bhatnager, editor. Metallic and Semiconducting Glasses, Switzerland: Trans Tech Publ. 1987, 749-59.

[26] Whang SH, Polk DH, and Giessen BC. Hardness vs. Young's modulus of metallic glasses. In: Masumoto T, Suzuki K, editors. Rapidly Quenched Metals, Sendai: The Jpn Inst Metals. 1982, 1365-8.

[27] Y. Wua, H. Wang , H.H. Wua, Z.Y. Zhang , X.D. Hui , G.L. Chen , D. Ma, X.L. Wang , Z.P. Lu, Formation of Cu–Zr–Al bulk metallic glass composites with improved tensile properties, Acta Materialia. 2011, 59: 2928–2936.

[28] Hofmann DC, Suh JY, Wiest A, Duan G, Lind ML, Demetrious MD, Nature. 2008, 451:1085.

[29] Hofmann DC, Suh JY, Wiest A, Lind ML, Demetriou MD, Johnson WL. Proc Natl Acad Sci, USA. 2008, 105: 20136.

[30] N.S. Barekara, S. Paulya, R.B. Kumarb, U. Kühna, B.K. Dhindawc, J. Eckerta, Structure–property relations in bulk metallic Cu–Zr–Al alloys, Materials Science and Engineering A. 2010, 527: 5867–5872.

[31] Argon, Plastic Deformation in Metallic glasses, Acta Materialia. 27: 47-58.

[32] Spaepen F, A microscopic mechanism for steady state inhomogeneous flow in metallic glasses, Acta Materialia. 1977, 25: 407-415.

[33] Morrel H. Cohen and David Turnbull, Molecular Transport in Liquids and Glasses, Journal of Chemical Physics. 1959, 31: 1164- 1169.

[34] Nieh, Wadsworth, Homogeneous behavior of bulk metallic glasses, Scripta Materialia. 2006, 54: 387–392.

[35] A.L. Mulder, R.J.A. Derksen, J.W. Drijver, S. Radelaar, Creep and tensile behaviour of $Fe_{40}Ni_{40}B_{20}$ at elevated temperatures, Sendai, Japan Institute of Metals, Sendai, Japan. 1982, 1345–1348.

[36] Y. Kawamura, T. Nakamura, A. Inoue, Superplasticity in $Pd_{40}Ni_{40}P_{20}$ Metallic Glass, Scripta Mater. 1998, 39: 301–306.

[37] V.A. Khonik, V.A. Zelenskiy, High- temperature ductility and superplasticity of metallic glasses ,Phys Met Metall. 1989, 67: 196-201.

[38] W. H. Jiang, F. X. Liu, D. C. Qiao, H. Choo, P. K. Liaw, R. Li, and T. Zhang, Effects of Temperatures on Inhomogeneous Plastic Flows of a Bulk-Metallic Glass, Advanced Engineering Materials. 2008, 10: 11.

[39] A. Inoue, X.M. Wang and W. Zhang, Developments and Application of Bulk metallic glasses, Rev.Adv.Mater.Sci. 2008, 18: 1-9.

[40] N. Yedla, Deformation behavior of ribbons of Copper-Zirconium based metallic glass with nanocrystalline precipitates-classical molecular dynamics and experimental studies, Ph.D thesis (2013), Department of Metallurgical and Materials Engineering, Indian Institute of Technology Kharagpur.

[41] Lu, Ravichandran, Johnson, Deformation behavior of the $Zr_{41.2}Ti_{13.8}Cu_{12.5}Ni_{10}Be_{22.5}$ bulk metallic glass over a wide range of strain-rates and temperatures, Acta Materialia. 2003, 51: 3429–3443.

[42] Shin Takeuchi, Keiichi Edagawa, Atomistic simulation and modeling of localized shear deformation in metallic glasses, Progress in Materials Science. 2011, 56: 785–816.

[43] Mirim Lee, Chang-Myeon Lee, Kwang-Ryeol Lee, Evan Mad, Jae-Chul Lee, Networked interpenetrating connections of icosahedra: Effects on: shear transformations in metallic glass, Acta Materialia. 2010.

[44] Kazutaka Fujita, Junji Ohgi, Vasek Vitek, Tao Zhang and Akihisa Inoue, Molecular Dynamics Simulation on Anelasticity under Tensile and Shearing Stresses in Single Component Amorphous Metal, Materials Transactions. 2005, 46: 2875 - 2879.

[45] Wilfred Gunsteren and Herman Berendsen, Computer Simulation of Molecular Dynamics: Methodology, Applications, and Perspectives in Chemistry.

[46] www.lammps.sandia.gov

[47] Michael P. Allen, Introduction to Molecular Dynamics Simulation, John von Neumann Institute for Computing, J ulich, NIC Series. 2004, 23: 1-28,.

[48] Q. Spreiter and M Walter, Classical molecular dynamics simulation with the velocity verlet algorithm at strong external magnetic field.

[49] Charles Francis Vardeman, Computational Study of Metallic Glasses and Nanoparticles, PhD thesis, Graduate School of the University of Notre Dame.

[50] Daw, M. S., Baskes, Embedded-Atom Method - Derivation and Application to Impurities, Surfaces, and Other Defects in Metals, Physical Review. 1984, 29: 6443-6453.

[51] H. Bekker, Molecular Dynamics Simulation Methods**,** Thesis Rijksuniversiteit Groningen. - With ref. ISBN 90-367-0604-1.

[52] Mayur Suri, Phase-Transition Assisted Deposition of Passivated Nanospheres, Master thesis, Graduate School of the University of Minnesota.

[53] Humphrey, W., Dalke, A., Schulten, VMD: Visual molecular dynamics, Journal of Molecular Graphics & Modelling.1996, 14: 33-38.

[54] D. Sopu, Y. Ritter, H. Gleiter, and K. Albe, Deformation behavior of bulk and nanostructured metallic glasses studied via molecular dynamics simulations, Physical Review. 2011, 83:100202(R)